

12-2013

Piezoelectric bedload impact sensor (PBIS) for particle size distribution.

Jeong Won Park 1977-
University of Louisville

Follow this and additional works at: <https://ir.library.louisville.edu/etd>

Recommended Citation

Park, Jeong Won 1977-, "Piezoelectric bedload impact sensor (PBIS) for particle size distribution." (2013). *Electronic Theses and Dissertations*. Paper 1095.
<https://doi.org/10.18297/etd/1095>

This Doctoral Dissertation is brought to you for free and open access by ThinkIR: The University of Louisville's Institutional Repository. It has been accepted for inclusion in Electronic Theses and Dissertations by an authorized administrator of ThinkIR: The University of Louisville's Institutional Repository. This title appears here courtesy of the author, who has retained all other copyrights. For more information, please contact thinkir@louisville.edu.

PIEZOELECTRIC BEDLOAD IMPACT SENSOR (PBIS)
FOR PARTICLE SIZE DISTRIBUTION

By

Jeong Won Park
B.S., University of Louisville, 2002
M.Eng., University of Louisville, 2007

A Dissertation
Submitted to the Faculty of the
J.B. Speed School of the University of Louisville
In Partial Fulfillment of the Requirements
For the Degree of

Doctor of Philosophy

Department of Civil and Environmental Engineering
University of Louisville
Louisville, Kentucky

December 2013

Copyright 2013 by Jeong Won Park

All rights reserved

PIEZOELECTRIC BEDLOAD IMPACT SENSOR (PBIS)
FOR PARTICLE SIZE DISTRIBUTION

By

Jeong Won Park
B.A., University of Louisville, 2000
M.Eng., University of Louisville, 2007

A Dissertation Approved on

November 8, 2013

by the following Dissertation Committee:

Dissertation Director
Dr. Arthur C. Parola

Dr. Mark N. French

Dr. Thomas D. Rockaway

Dr. David A. Howarth

ACKNOWLEDGMENTS

I would like to express appreciation to my advisor, Dr. Arthur C. Parola, who introduced me the issues and demands associated with this research topic. Without his supervision and financial support this dissertation would not have been possible.

I would like to thank my committee members, Dr. Mark N. French, Dr. Thomas D. Rockaway in the department of civil and environmental engineering and Dr. David A. Howarth in the department of geography and geoscience. Without their comments and editing this dissertation would not have been completed.

I would like to thank Douglas J. Jackson, an electronics research engineer in the department of electrical and computer engineering. Without his countless assistance and suggestion based on his expertise in electrical engineering this research would not have been valuable.

I would like to thank Dr. William M. McGinley in the department of civil and environmental engineering. Without his comments and advice in the experimental design and set-up it would have been difficult to state the limitations of this research.

I would like to thank Dr. Patricia A. Cerrito, my former committee member and a former professor in the department of mathematics. She inspired me in statistical data analysis until passing away 2 years ago in August 23, 2011.

I would like to thank Dr. Donald. J. Hagerty, a former professor in the department of civil and environmental engineering, who encouraged and guided me to pursue a PhD degree continuously in the University of Louisville.

I would like to thank Bernie D. Miles, Thomas M. Carroll and Gary E. Graf for their interdepartmental technical support for this research. Without their technical knowledge and skills any equipment for this research would not have been ready yet.

ABSTRACT
PIEZOELECTRIC BEDLOAD IMPACT SENSOR (PBIS)
FOR PARTICLE SIZE DISTRIBUTION

Jeong W. Park

November 8, 2013

A multi-channel Piezoelectric Bedload Impact Sensor (PBIS) is developed to estimate mass and particle-size distribution of bedload in low to moderate slope natural streams. The PBIS's stand-alone design with a sufficiently large data memory facilitates continuous long-term monitoring for low-scale bedload measurements. The design concept of PBIS is based on a hypothesis that particle collision energy on the PBIS plate increases with hydraulic energy and particle size. Thus, particle size can be differentiated by the number of impulses registered in four different threshold channels. The feasibility of PBIS was evaluated by developing a calibration model based on laboratory flume experiments. Two different types of experiment were conducted: (1) individual particle experiment and (2) multi-size particle experiment. The individual particle experiment results indicated that hydraulic condition affected the mode of bedload particle motion. The mean impulse rate per particle is expressed as a function of bed shear stress, τ . In addition, the represented particle sieve size range of each threshold channel was determined based on the fractional impulse ratio per unit mass by the particle sieve size class. The multi-size particle experiment results indicated that multi-particle interaction and signal interference from consecutive particle impacts on the PBIS plate caused a notable reduction of registered

impulses in channel 1 from approximately 700 impulses per minute. The bias between individual and multi-size particle experiment results caused by multi-particle effects were expressed by a function of bed shear stress, τ , and mean impulse rate, R_j , in each PBIS threshold channel. The adjusted calibration coefficient is a coefficient of linear equation to convert registered impulses to mass of particles retained in the represented particle sieve size classes of each channel. The adjusted calibration coefficients for each channel were estimated using the two-dimensional response surface methodology (RSM) with two variables, bed shear stress, τ , and mean impulse rate, R_j . This study was enough to show the feasibility of the multi-channel PBIS to obtain mass and particle-size distribution of small gravel bedload. However, many issues associated with the calibration model are still remained beyond this study. First of all, the calibration model was developed based on laboratory flume experiments conducted in a well-controlled small-scale environments. Second, from the comparison between the actual and the estimated values, it was found that two inherent error factors which can cause overestimate are imbedded in the linear calibration model of PBIS. Third, two major assumptions for the model, an equal fractional bedload particle-size distribution and the law of large number, always have a distinction from chaotic phenomena in natural bedload transport. Because of that, the most preferential request will be the field application.

TABLE OF CONTENTS

	PAGE
ACKNOWLEDGEMENTS.....	iii
ABSTRACT.....	v
TABLE OF CONTENTS.....	vii
LIST OF TABLES.....	viii
LIST OF FIGURES.....	x
CHAPTER I INTRODUCTION.....	1
CHAPTER II EQUIPMENTS AND MATERIALS.....	9
CHAPTER III EXPERIMENT.....	24
CHAPTER IV RESULT.....	28
CHAPTER V ANALYSIS.....	44
CHAPTER VI CONCLUSION.....	68
REFERENCES.....	70
APPENDIX.....	73
CURRICULUM VITA.....	76

LIST OF TABLES

TABLE		PAGE
Table 1.	Summary of specifications of experimental hydraulic conditions.....	16
Table 2.	Half-phi (ϕ) scale sediment sieve size ranges used for individual particle experiments (solid line) and multi-size particle experiments (dashed line) are indicated by the boxed bold lines	23
Table 3.	Experimental matrix	27
Table 4.	Summary of the individual particle experiment results	34
Table 5.	Predicted impulses for 600g multi-size gravel sample according to the individual particle experiment	38
Table 6.	Summary of the multi-size particle experiment results and comparison with the predicted mean impulses calculated based on the individual particle experiment results	41
Table 7.	Upper and lower boundaries of represented sieve size classes of each channel in three experimental hydraulic conditions	51
Table 8.	Calibration coefficients from the individual particle experiments in three experimental hydraulic conditions	54
Table 9.	Adjusted calibration coefficient matrix for channel (a) 1 and (b) 2 (3 experimental hydraulic conditions \times 3 designed sediment-feeding rates)	60

Table 10.	Goodness of fit	61
Table 11.	Estimate error of bedload quantity	64

LIST OF FIGURES

FIGURE		PAGE
Figure 1.	Three distinct components of “sediment system” in gravel-bed streams. (a) bed surface layer (armor), (b) substrate and (c) bedload (Pitlick, Cui, and Wilcock, 2009).....	1
Figure 2.	Multi-channel PBIS.....	10
Figure 3.	Geometric physical dimensions and signal detection hardware layout for the multi-channel PBIS.....	11
Figure 4.	Schematic view of electric components in multi-channel PBIS.....	12
Figure 5.	Typical output signal of individual particle impact.....	13
Figure 6.	Average peak voltage output of each particle size.....	13
Figure 7.	Schematic view of experimental equipment set-up.....	14
Figure 8.	Multi-channel PBIS installed on the flume bed 2.67m downstream from sediment-feeding location.....	16
Figure 9.	(a) Longitudinal profiles of experimental flows and flume, (b) Water surface slopes of experimental flows above PBIS	17
Figure 10.	Pit-trap (bucket) sampler installed in Harrison Fork.....	18
Figure 11.	Comparison of mean particle mass for sieve sizes in a half-phi(ϕ) increments for square-hole sieves between test gravel and sediment in Squaw Creek, MT. (Bunte and Abt, 2001)	19

Figure 12.	Comparison of mean particle registration rate by retaining sieve sizes in three different hydraulic conditions.....	29
Figure 13.	Definition sketch of particle saltation (Rijn, 1984)	31
Figure 14.	Mean impulses by particle retaining sieve size class in three different hydraulic condition (Bed shear stress = (a) 38.0 Pa, (b) 28.7 Pa and (c) 19.5 Pa).....	33
Figure 15.	Comparison between the predicted and the estimated mean impulses per minute for equal size-fraction gravel sample in each channel ((a) $j = 1$, (b) 2, (c) 3 and (d) 4)	39
Figure 16.	Mean number of particles per unit mass (= 1 g) for retaining sieve sizes....	46
Figure 17.	Comparison between the mean impulses per 1 g unit mass and one impulse per particle line in each channel ((a) $j = 1$, (b) 2, (c) 3 and (d) 4)	47
Figure 18.	Cumulative and relative mean impulse frequency distribution of equal size-fraction gravel sample in each channel ((a) $j = 1$, (b) 2, (c) 3 and (d) 4)	49
Figure 19.	Calibration coefficient for the represented particle sieve size range in three experimental hydraulic conditions ((a) $j = 1$ and (b) 2)	55
Figure 20.	Bias of the predicted mean impulse from the estimated mean impulse changes by the mean designed sediment-feeding rate and BSS ((a) $j = 1$ and (b) 2)	56
Figure 21.	Response surface model for channel 1 (a) contour, (b) surface and (c) residual plots	62
Figure 22.	Response surface model for channel 2 (a) contour, (b) surface and (c) residual plots	63

Figure 23. Comparison between mean designed sediment transport rate of multi-size particle sample and estimated sediment transport rate using the bedload estimate model for the multi-channel PBIS65

Figure 24. Comparison of cumulative particle-size distribution of equal size-fraction experimental sediment sample with estimated particle-size distributions in three hydraulic conditions ($\tau =$ (a) 19.5 Pa, (b) 28.7 Pa and (c) 38.0 Pa)...67

CHAPTER I. INTRODUCTION

Sediment transport of particles which composes the streambed of natural gravel-bed channel is usually classified by two different ways, source of sediment particles and sediment transport mechanism (Wilcock, Pitlick, and Cui, 2009). However, the separation as three components of the sediment system in Figure 1 might be appropriate to interpret the frequency of mobility of coarse sediment in gravel-bed stream. The three components are large surface armor material, comparatively smaller substrate materials and bedload (Pitlick et al., 2009). Armor materials such as boulders (> 256 mm in a length of intermediate axis of particle) and cobbles (> 64 mm) are comparatively immobile against high stress flow. Thus, they provide stable grade controls of longitudinal streambed profile

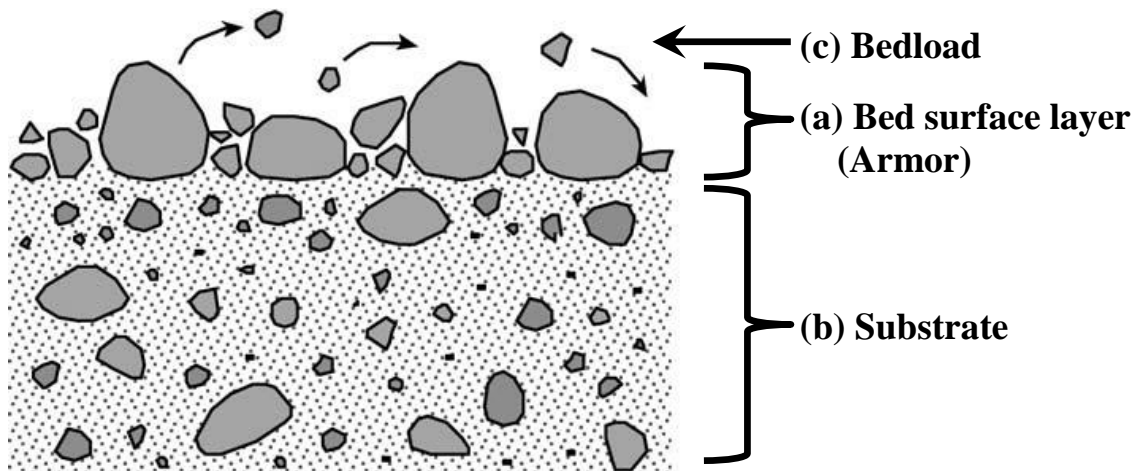


Figure 1. Three distinct components of “sediment system” in gravel-bed streams. (a) bed surface layer (armor), (b) substrate and (c) bedload (Pitlick et al., 2009)

and limit of bedload supply from substrate. On the contrary to armor, bedload is transported much more frequently than armor material. However, the boundary between armor and bedload is not clearly distinguished by the size of sediment particles because the definition of bedload is based on sediment transport mechanism. The definition of bedload is particles transported by rolling, sliding or saltating (hopping or jumping) along the stream bed in flowing water. According to the definition of bedload, either armor material or finer substrate material also can be bedload depending on the strength of hydraulic force although the occurrence is comparatively rare and the fraction in total mass of bedload might be also small in the stable channel bed (Diplas, Kuhnle, Gray, Glysson, and Edwards, 2008). It was observed that the median particle size of bedload fell within ± 1 phi sieve class interval of that of the subsurface material in high bedload transport rate when armor and substrate materials were in motion in high flow condition (Gomez and Church, 1989). Therefore, the recurrence rate of excessive bedload supply from substrate caused by disturbance of the armor layer can be interpreted into the degree of stability of the channel bed.

A popular speculation in sediment transport study is that bedload is generally a small fraction of total sediment transport load (about 10 %) although the temporal and spatial variations of bedload are very high (Meade, Yuzyk, and Day, 1990; Hayward, 1978). Bedload mainly occurs in limited low order gravel-bed streams during a comparatively short period. However, the absolute quantity of bedload produced and transported during few low-frequency high flow events is not negligible. Hayward's field observation showed that 10 of 81 storm events (about 1 % of total time) produced 90 % of the total sediment. The quantity of bedload supply was more than 100 metric tons for a 5 year observation

period. In addition, the quantity of bedload transport is more dependent on a supply of sediment than on the sediment transport capacity calculated by hydraulic condition. (Hayward, 1978). Therefore, bedload management plans for episodic bedload transport in mountain or low-order streams require an approach in terms of frequency as well as magnitude.

The importance of bedload management is due to that the stability of the variable boundary of natural streams is associated with flow regime in stream and riparian zone. Alteration of flow regime due to deposition (aggradation) / incision (degradation) in unwanted area causes damage to not only human residence but also biotic habitat in the local stream reach. The disturbance of habitat and the change of ecological function by excessive bedload can directly or indirectly threaten invertebrates residing in substrate and eventually lead to the population decline of invertebrates in the stream. Some ecological research results show that the stability of stream substrate interpreted by intensity and frequency of bedload transport is strongly related to the population of invertebrates in gravel-bed streams (Pitlick and Wilcock, 2001). Thus, bedload management and stream stabilization is usually in the core of stream restoration projects targeted to restore aquatic habitats (Cantrell, Schwartz, and Barry, 2009; F. Douglas Shields, Copeland, Klingeman, Doyle, and Simon, 2003).

Despite the long history of efforts to characterize the spatial and temporal fluctuations and competence of bedload transport, it is still difficult to estimate sediment transport accurately (Khorram and Ergil, 2010; Gomez and Church, 1989). That is not only due to the natural complexity of bedload transport phenomenon including the variable sediment-supply issue mentioned in the second paragraph of this chapter but also a gap

between applicable and requisite data (Gray and Simões, 2008; Papanicolaou, Elhakeem, Krallis, Prakash, and Edinger, 2008). Long-term bedload transport data with sufficient resolution is necessary to elucidate the linkage between hydraulic and sedimentological data, but it has been obtained from a few limited stream sites and flume experiments (Gray and Simões, 2008; Gomez, 1991; Gomez and Church, 1989). It is due to that the collection of high-quality data is an expensive and time-consuming task (Gomez, 2006).

There have been many efforts to interpret the mechanism and determine the quantity of bedload for more than a century theoretically and empirically (Gomez, 1991). In the meantime, many different types of bedload samplers have been developed for bedload research (Diplas et al., 2008). Even though the direct bedload sampling methods have unique advantages and are still useful, they are unsuitable for the popular demand of continuous measurement in a wide range of areas to characterize temporal and spatial variation of bedload transport rates (Gray, Laronne, and Marr, 2010; Diplas et al., 2008). To make up for the deficiency of the direct bedload sampling, new sampling techniques were developed and new sampling devices were renovated (Diplas et al., 2008; Ryan, Bunte, and Potyondy, 2005). However, as a matter of type of direct bedload samplers, a common issue has been always that the cost of either equipment or operation in order to collect bedload sample continuously with high-resolution for a long-term period is expensive. In spite of the deficiency, the direct sampling methods have been popularly being used till today, for they allow to perform particle-size distribution analysis for bedload sample obtained from the direct samplers.

To overcome the deficiency of direct methods, indirect bedload-surrogate measurement apparatuses have been developing since the 1930s (Richards and Milne, 1979;

Johnson and Muir, 1969; Anderson, 1976; Hubbell, 1964). The early indirect bedload measurement apparatuses are acoustic sensors to convert sonar signals produced by interparticle or particle-instrument collisions to electric current or voltage signals. The main problems of indirect methods with the acoustic bedload sensors were a dearth of high resolution data storage and a limitation of stream flow noise reduction process (Johnson and Muir, 1969). Since the earliest acoustic bedload sensors were developed, great advances in physical technology of electric device and analytical signal process have been accomplished. However, the indirect acoustic techniques are still under restrictions of practical application in field measurement due to complexity in operation and analysis (Møen, Bogen, Zuta, Ade, and Esbensen, 2010; Richards and Milne, 1979). In the operation of acoustic bedload measurement devices, calibration is a difficult and expensive process which requires a highly-trained analytical technique (Møen et al., 2010). Even though calibration is an essential process for all types of indirect devices, calibration of acoustic devices to deal with electric analog signals might be the biggest restriction in practical field measurements.

The piezoelectric bedload impact sensor (PBIS) is one of popular acoustic bedload measurement devices. Bedload measurement with the earliest model of PBIS was conducted since autumn 1986 in the Erlenbach catchment of central Switzerland. The earliest model of PBIS was not distinguished from hydrophone and called the same name. However, since then the PBIS recorded the counts of electric impulse generated by particle collisions on the sensor plate regardless of particle size in contrast with common acoustic bedload measurement devices recording raw electric analog signals (Bänziger and Burch, 1990). By digitizing analog signals and recording as the number of impulses, PBIS required

comparatively simple data analysis rather than other acoustic devices. In the calibration of PBIS based on long-term observation, well-fitted linear relationships were derived between the number of impulses and the sediment volume accumulated in the downstream sediment basin during sediment transport events (Rickenmann and McArdell, 2007, 2008). Even after replacing a piezoelectric crystal with a geophone, a linear correlation between the number of impulses and the sediment volume seems consistent (Rickenmann, Turowski, Fritschi, Klaiber, and Ludwig, 2012). Yet the advantage of digitized signal of PBIS is not intended to undermine the inherent value of raw electric analog signal. The greatest advantage of recording electric analog signal from acoustic sensors is the compatible transformation depending on diverse purposes of application, such as frequency-domain analysis to determine the size distribution of bedload particles and remove noise or fault signals (Møen et al., 2010).

With recent advances in electric technology, a stand-alone design of acoustic bedload sensor was developed to obtain high-resolution bedload transport rate data (Richardson, Benson, and Carling, 2003). The stand-alone sediment impact sensor adopted the functional concept of PBIS and additionally facilitated installation and operation in bedload measurement by reducing the physical size of the data logger. On the practical aspect of indirect bedload measurement, this sediment impact sensor accomplished great strides because the practical design allows economic bedload measurements in a wide range of purposes and scales. However, there are still three main constraints of its functionality: (1) insensitivity of detecting small gravels, (2) small data memory, and (3) no information for particle-size distribution. The sediment impact sensor was comparatively insensitive to detect small gravels dominant in low to moderate slope

channel beds. The memory size is also very small for high-resolution long-term measurement. The 8-bit data memory system allows the maximum 256 impulses in a sampling interval and the capacity of memory is saturated in about 11.2 days with 1-minute sampling interval. Above everything else, the great constraint of functionality is that spatially and temporally variable particle size distribution and competence of bedload transport cannot be provided.

Engineers, scientists and river managers have emphasized the necessity of reliable bedload transport measurement apparatuses and techniques for many different purposes (Gray et al., 2010; Schwendel, Death, and Fuller, 2010; Gomez, 1991). The current demands reported from the 2002-2007 sediment-technology workshops focus on new bedload measurement technologies enhancing local-scale bedload research and monitoring for river management and restoration purposes (Gray et al., 2010). The most notable requested information from new bedload measurement devices is particle size distribution of bedload. That is another main reason for the continuous necessity of direct bedload measurement devices except as a means for calibrating indirect bedload measurement devices. Thus, there are many efforts to develop and calibrate indirect bedload measurement devices which can provide particle size distribution of bedload in addition to estimating bedload transport rate with high-resolution data. As a part of the research trend, a stand-alone PBIS which has four different sensitivity channels to response to the strength of sediment particle impact was developed. The design concept of multi-channel PBIS is based on a hypothesis that the strength of particle impact is proportional to the size of particle. The purpose of this research is to evaluate the functionality of a multi-channel

PBIS by developing a calibration model to estimate mass and particle size distribution of bedload based on laboratory flume experiments.

CHAPTER II. EQUIPMENT AND MATERIALS

All experiments for this research were conducted in an open channel laboratory flume specifically modified for this work. This section specifies the experimental equipment and materials used for the flume experiments. There are 3 components described: (1) multi-channel particle bedload impact sensor (PBIS); (2) open channel flume; (3) test gravel materials.

1. Multi-channel PBIS – A four-channel PBIS was developed to detect bedload pebbles with a size range from 4 mm to 63 mm in low to moderate slope (~ 2%) headwater streams. Each particle impact detected by the PBIS generates an electrical signal and the signal series form the basis to develop a relationship indicating the size-fraction of bedload particles. The four-channel PBIS has a typical shape modified from existing single-channel type PBIS. A one-dimensional accelerometer is mounted under 6.4 mm (1/4 inches) thick 0.18 by 0.20 m (7 by 8 inches) stainless steel plate. A 0.11 m (4.5 inches) diameter and 0.15 m (6 inches) tall watertight stainless steel cylindrical housing is welded under the center of the plate, which secures electrical components including the accelerometer as shown in Figures 2 and 3. Figure 2 is the actual device developed for this work and the device is mounted in the streambed with the cylindrical portion buried below bed level such that the plate is flush with streambed. Figure 3 shows a schematic diagram of the PBIS showing the geometric physical dimensions and the location of the electrical signal detection and processing hardware.



Figure 2. Multi-channel PBIS

The multi-channel PBIS is composed of five main components. An accelerometer installed on the bottom of the PBIS plate responds to mechanical vibration caused by collisions (impacts) of coarse sediment with the top plate and converts the mechanical energy into an electrical energy signal or impulse. The one-dimensional accelerometer generates an alternative voltage wave form proportional to the strength of the force applied to the plate by the sediment collision (impact). The one-dimensional accelerometer was selected with sensitivity to detect gravel size particles from 4 mm to 63 mm. There may be a large variation in particle size-fraction in typical bedload materials depending on the intensity of the bedload transport flow events and the availability of sediment supply in a stream. However, based on field monitoring data analysis from the test gravel sampling sites, coarse sediment collected in pit-trap bedload samplers mostly falls within this detectable particle size range. The detectable particle size range of the multi-channel PBIS will be discussed later in this document. The detectable particle size range of each PBIS

channel is not only related to the sensitivity of the accelerometer but also to the hydraulic and geomorphologic properties of the stream, which can influence the mode of bedload particle motion.

The accelerometer generates a voltage analog signal when a particle impact is occurred. The accelerometer signal is amplified and depending on the signal strength or amplitude, one or more of the four voltage threshold switches are independently closed. The threshold switch is closed when the magnitude of the amplified voltage signal exceeds the preset threshold of each channel. A counter records the number of impulses for each threshold switch and a data logger stores the records for later retrieval. The entire process from particle impact and electronic signal generation to data recording are summarized in Figure 4.

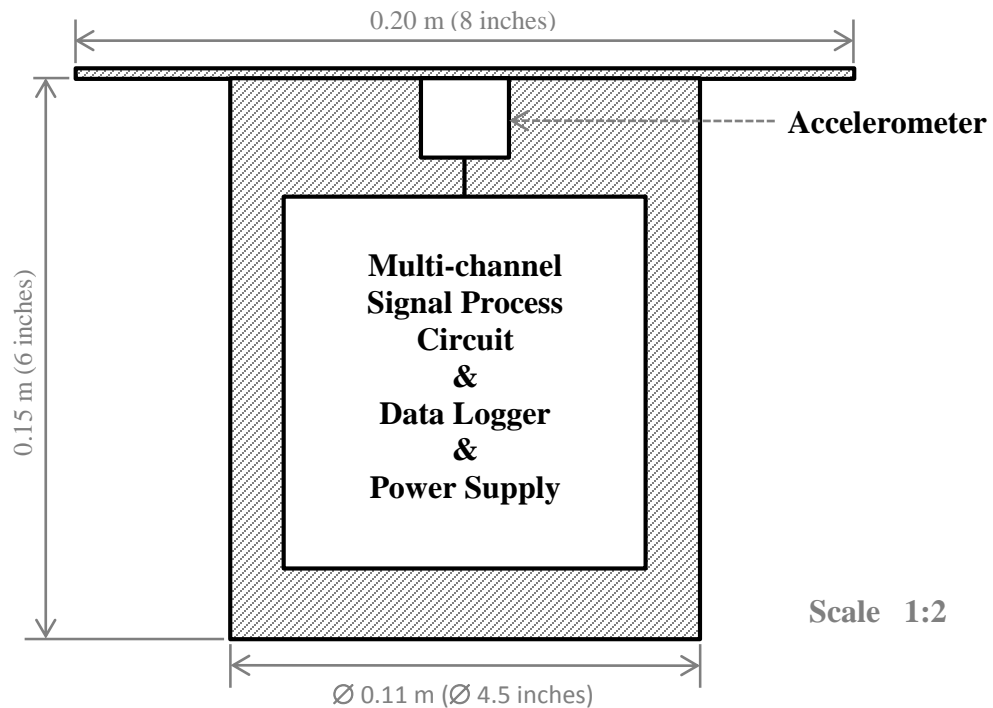


Figure 3. Geometric physical dimensions and signal detection hardware layout for the multi-channel PBIS

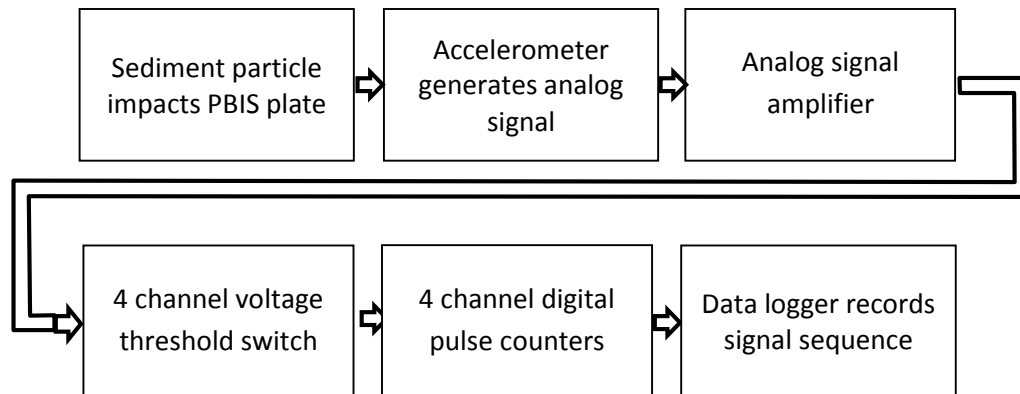


Figure 4. Schematic view of electric components in multi-channel PBIS

A sample particle impact signal sequence and the threshold or detection limit level for each of the 4 switches is shown in Figure 5. When the signal voltage oscillation diminishes below the threshold of any activated switch, the switch automatically resets. The voltage threshold of each channel is empirically designed to detect two particle size classes from 8 mm to 63 mm in a half ϕ -scale particle classification. The threshold level was determined from preliminary experiment results to discern the minimum particle size required to activate each channel. The results of the preliminary experiments using gravel particles to define the sensor channel threshold levels are displayed in Figure 6. The channel thresholds were defined to be evenly distributed over the functional range of the accelerometer. The digital pulse counter for each channel independently counts the number of digitized impulses generated by each voltage threshold switch. The total number of impulses from each channel are stored in a data logger with a common recording time interval. Eventually, the complex analog wave signal is digitized and recorded as a positive integer at the associated sampling time interval.

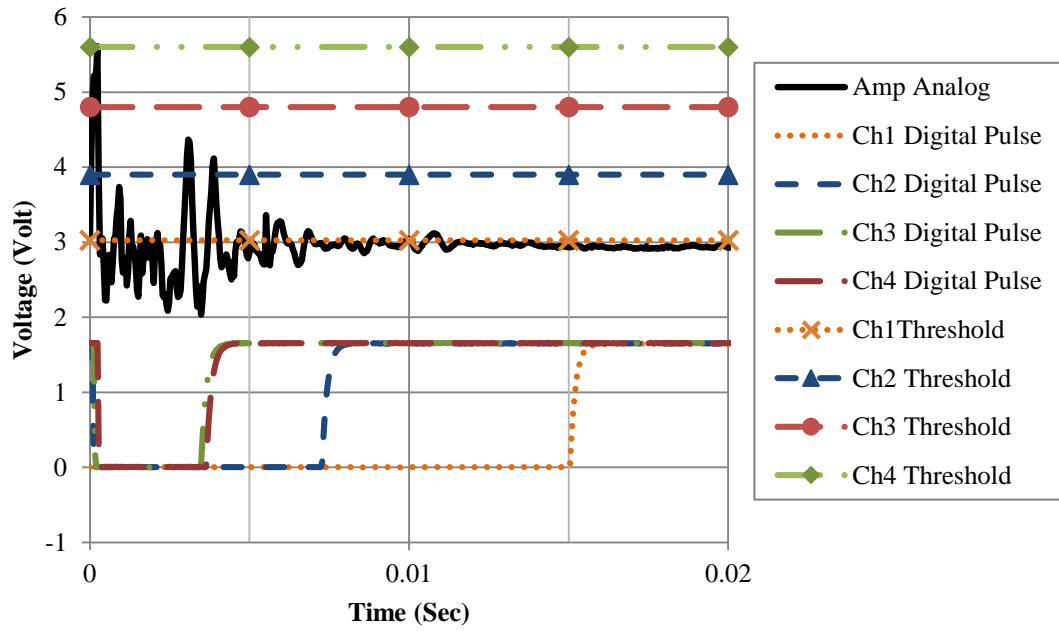


Figure 5. Typical output signal of individual particle impact

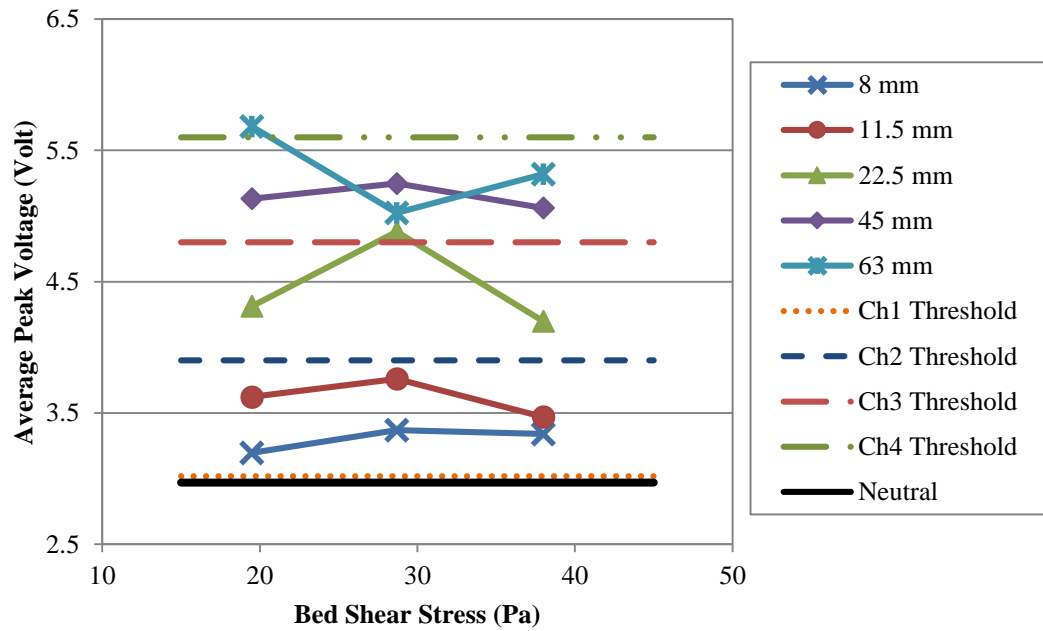


Figure 6. Average peak voltage output of each particle size

2. Open channel laboratory flume – The open channel flume is a recirculating flume and consists of three main parts and two auxiliary parts. The upstream reservoir (headbox), flume channel, and sediment collection box (tailbox) are the main stationary parts of the open channel flume, as shown in Figure 7. The gravel-feeding funnel and water tank for the PBIS are the auxiliary components. The water recirculation system including a sump, piping network and variable speed pump are part of the system but not included in the schematic view.

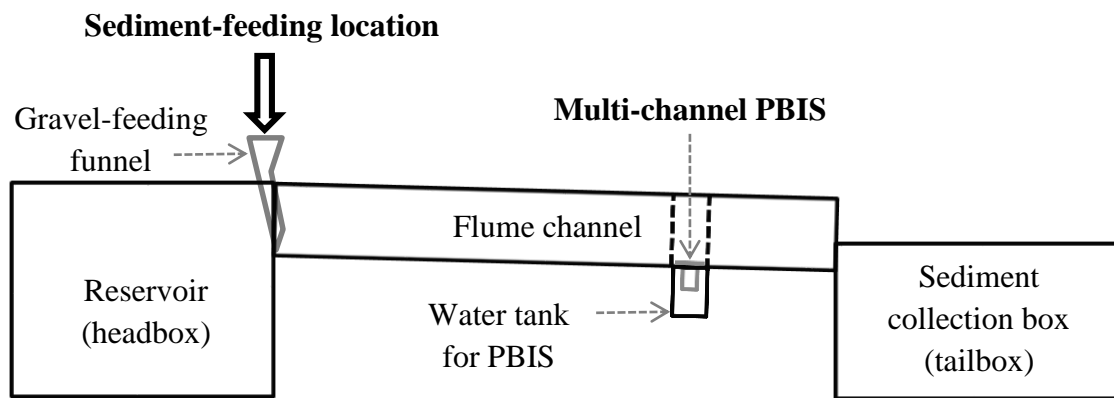


Figure 7. Schematic view of experimental equipment set-up

The two auxiliary components were specifically designed for these experiments. Ideally, the PBIS accelerometer responds only to particle impact vibrations generated on the PBIS plate, but it was found that secondary vibrations from the waterproof housing were enhanced when the housing was exposed to the open air while mounted under the flume. To diminish secondary vibration effects, a below grade water tank was constructed to surround the PBIS cylindrical waterproof housing that contains the electronic sensors and data recorders. This is comparable to in-situ field conditions where the entire PBIS housing is buried in the streambed material and surrounded by water.

The gravel-feeding funnel is used to introduce test particles smaller than 32 mm directly into the flowing water near the flume channel bed. The funnel was necessary since when these small particles were fed from above the water surface, a comparatively large percentage of the particles passed completely across the PBIS plate without impact. This led to an unacceptable high non-detection rate or missing particle errors. Feeding sediment particles directly to the flume bed was useful to mimic a more natural mode of bedload particle transport and motion along the channel bed.

The flume is wood-framed with length, width and height dimensions of approximately 3.7 m (12 ft.) long, a width of 0.20 m (8 in.) by depth of 0.40 m (15 5/8 in.) at maximum cross-sectional area and 1.9% average slope in the channel section location of the PBIS. The PBIS is installed 2.67 m (8 3/4 ft.) downstream of the reservoir and set inside a 0.15 m (6 in.) diameter cylindrical water tank housing under the flume bed, as shown in Figure 7. The experimental flume was specially designed such that the longest dimension (0.20 m) of the PBIS plate fits flush with the width of flume, as shown in Figure 8. Long distance reach between the sediment-feeding location and the PBIS allows steady-state hydraulic flow conditions to form up- and down-stream of the sensor. In addition, sediment introduced upstream of the PBIS can be well mixed and distributed in water until reaching the PBIS section.

The experiments were conducted under 3 hydraulic conditions. The 3 hydraulic profiles are plotted in Figure 9 (a). All geometric profile data of the flume and water flows are obtained using optical surveying equipment. Water stages and water surface slopes of the 3 hydraulic flow conditions were measured based on geometric profiles in the steady-state hydraulic section above the PBIS as shown in Figure 9 (b). The mean discharge was

measured by a venturi meter installed in a section of recirculation pipe. The mean velocity was determined from the mean discharge and the cross-section area of water flow. All specifications of the 3 experimental hydraulic conditions are summarized in Table 1.



Figure 8. Multi-channel PBIS installed on the flume bed 2.67 m downstream from sediment-feeding location

Table 1. Summary of specifications of experimental hydraulic conditions

Experimental Hydraulic Condition	Mean Discharge (m ³ /s)	Mean Velocity (m/s)	Water Stage on PBIS (m)	Water Surface Slope	Mean Bed Shear Stress (Pa)
Low	0.030	1.4	0.11	0.019	19
Med	0.053	1.7	0.16	0.019	29
High	0.076	1.8	0.21	0.019	38

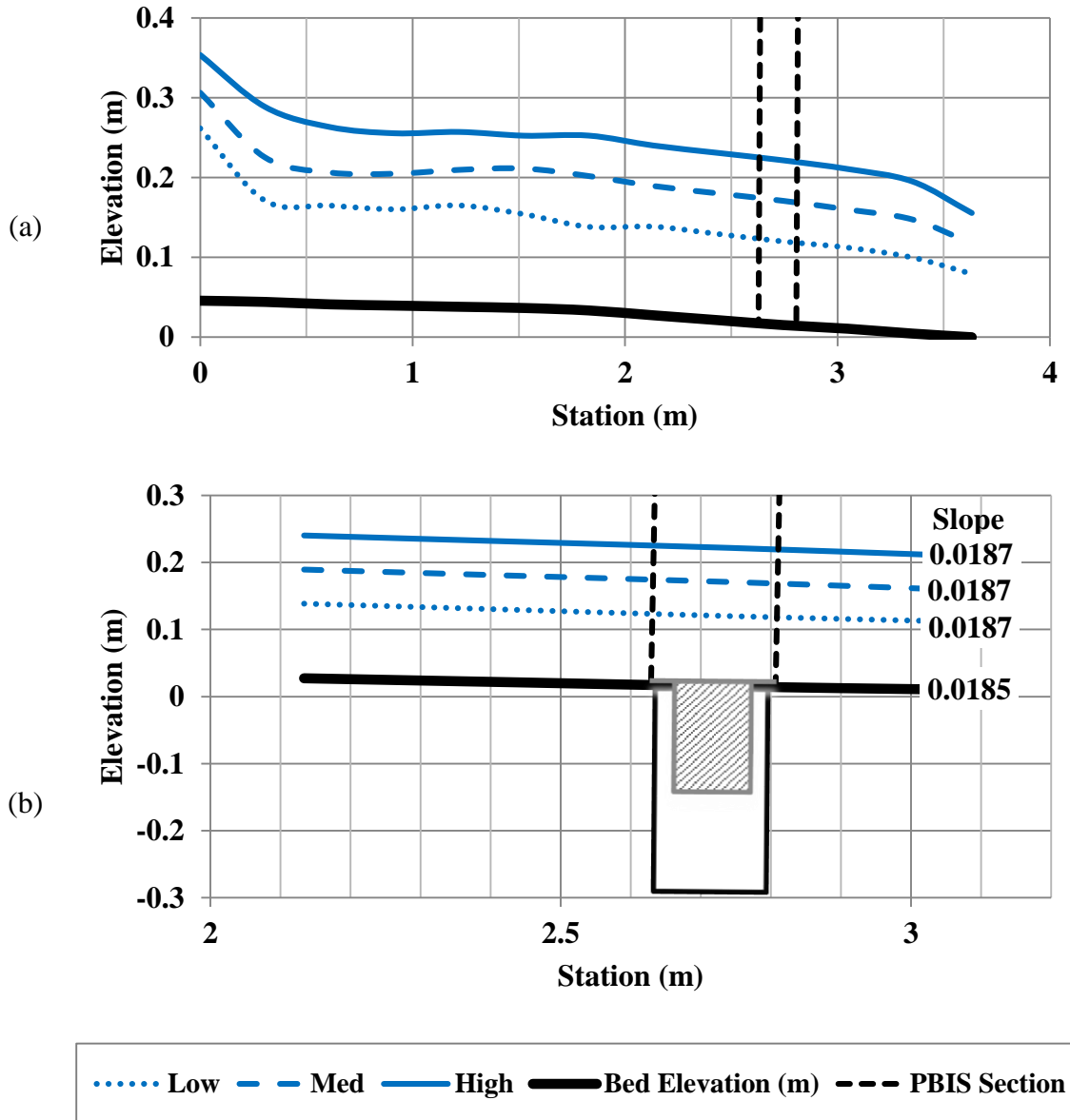


Figure 9. (a) Longitudinal profiles of experimental flows and flume, (b) Water surface slopes of experimental flows above PBIS

3. Test gravel – The test gravels are subsamples randomly selected by hand from bedload material samples captured in manual pit-trap (bucket) samplers during several events in Harrison Fork and Wilson Creek in Kentucky. Figure 10 shows the pit-trap bedload samplers installed in Harrison Fork. Gravels from the two alluvial streams are generally dolomite, limestone, and shale.



Figure 10. Pit-trap (bucket) sampler installed in Harrison Fork

Physical properties of sediment in natural channels can be characterized by many parameters such as density, bulk density, individual particle size and shape. Generally, individual sediment particles are physically characterized by the length of intermediate axis or the sieve size class in which a particle is retained. This is due to the practical difficulty of 3-dimensional measurement of many individual small particles and various irregular dimensions of larger particles. Thus, particle size appeared herein indicates particle retaining sieve size. However, gravel particles retained by a particle specific sieve size class have similarities to each other in average physical properties. As shown in Figure 11, mean particle mass has a significant correlation with the retaining particle sieve size class. Even in gravel collected from 2 different regional channels, similar mean particle mass is shown for each sieve size class. The coefficients of regression equation for test gravel collected from Harrison Fork do not exactly fall within the ranges of coefficient provided in a previous study. However, the difference of coefficients is comparatively small

although the two equations were developed based on different particle masses. Bunte et al (2001) used dry particle mass, whereas saturated particle mass was used to develop the particle mass-retaining sieve size correlation equation for test gravels (Bunte and Abt, 2001). The maximum difference of mean particle mass from the 2 sites is about 22 % at 63 mm sieve class. The largest potential difference of the intermediate axis of particles retained in the same sieve class can be a factor of 1 1/2 to 2 depending on the sieve size increment, either 1/2-phi (ϕ) or phi (ϕ) scale. The largest potential difference in the mass of particles retained in the same sieve class can be more than the size difference factor, depending on dimensions of particles aside from the intermediate axis.

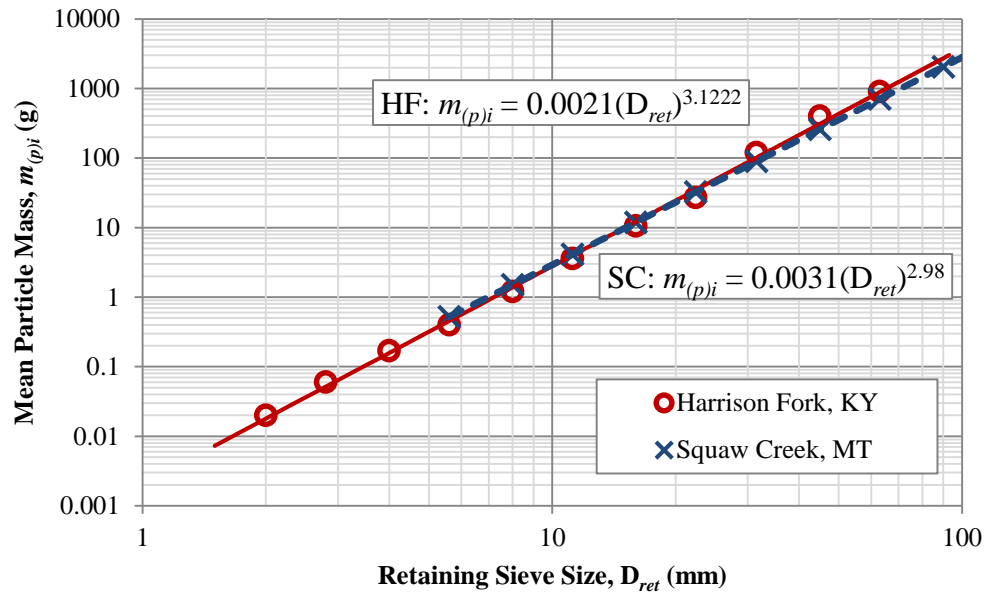


Figure 11. Comparison of mean particle mass for sieve sizes in a half-phi (ϕ) increments for square-hole sieves between test gravel and sediment in Squaw Creek, MT. (Bunte and Abt, 2001)

Neither the intermediate axis nor the sieve size class of sediment particle reflects the shape or three-dimensional size of particles. However, the shape of sediment particles, characterized by angularity and flatness factors, is as important a factor as the size or mass of particles in bedload transport because it influences the particle's movement in differing hydraulic conditions. Moreover, the movement of bedload particles such as rolling, sliding and saltating affects the strength of particle collision on the PBIS plate. Therefore, the particle shape is not a negligible factor for the calibration of a multi-channel PBIS since it differentiates particle size by the strength of particle collision impact on the sensor. Thus, particle shape is determined to be a random factor for this research and approached stochastically instead of using standard-size particles with a uniform dimension, such as glass marbles.

Test gravels used in experiments were not collected from one bedload transport event because a quantity of large test particles bigger than 32 mm from a single event was insufficient for the experiment. More than 40 particles in each sieve size class are required to define particle shape stochastically and necessary to satisfy the experiment matrix in Table 3 in chapter 3. In addition, it is important to have enough sediment to represent the characteristics of sediment in the sample region. The sediment sample region may include an entire upstream valley. Sample collection must also consider plans to eliminate sediment from a temporal dominant colluvial source in a single flow event. Size-classified test gravels are stored submerged in buckets, organized by sieve size class, and are completely saturated prior to and during experiments.

The size range of test gravels is determined by three limiting factors: (1) the smallest detectable particle size, (2) the smallest dimension of water flow cross-section,

and (3) a maximum sediment-feeding rate of 100 g/s per width of flume ($= 100 \text{ g/s}/0.2 \text{ m}$). The smallest particle size was determined using a series of preliminary particle detection tests. The particle detection test results are shown in Figure 12 in chapter 4. The general trend of particle registration rate increased with lower discharge and larger particle size. An average registration rate of approximately 16-25 % was observed with 4 mm particles in three flow conditions. The extended trend line of registration rate intercepts zero percent around 2.9 mm. Thus, the 4 mm retaining sieve size is the approximate lower boundary of detectable gravel particle for the PBIS.

The maximum particle size was controlled by the smaller dimension of the flume channel cross-section at the highest water flowrate. Water stage (depth) was the control for the maximum particle size at the two lower flow conditions, 0.11 and 0.16 m, whereas the width of the test flume, 0.20 m, was the control for high flow, 0.21 m. The average stage of high flow at 0.21 m is close to the 0.20 m width of the test flume. The maximum retaining sieve size for each hydraulic condition was determined under controlled conditions such that the potential maximum length of the intermediate axis of a particle retained in a sieve class was smaller than half of the controlling or limiting dimension for each hydraulic condition. This constraint on particle size is necessary in order that all particles are transported without interruption or disturbance from interaction with the flume structure. In addition, influence on hydraulic factors, such as slope, stage and velocity, by the presence of particles and particle movement within the flow can be minimized.

The last constraint on maximum particle size is applied only to the multi-size particle experiments. Three sediment-feeding rates in each hydraulic condition were implemented to simulate a range of bedload transport rates in natural channels. The largest

sediment-feeding rate, 100 g/s per width of flume ($= 100 \text{ g/s}/0.2 \text{ m} = 500 \text{ g/s/m} = 30 \text{ kg/min/m}$), in the multi-size particle experiment, rarely occurs except during low-frequency extreme events in natural channels. However, 500 g/s/m can be an instantaneous reading for a short sampling time interval, as short as one second, since a gravel particle in the 63 mm sieve being transported downstream in a second is detected as a 900 g/s load, (based on Figure 11). The variability of bedload transport rate over a sampling time interval may be high. However, in this controlled experiment test, the largest particle size is limited by the average mass of the particle size. The largest average individual particle mass in a multi-size sediment sample is 100 g, which corresponds to a 31 mm particle size. Therefore, the largest particle size for the multi-size particle experiment is 22.4 mm. In each sieve size class from 4 mm to 22.4 mm with a half-phi (ϕ) scale increment, 100 g of sediment is randomly sampled by hand and a 600 g multi-size sample is prepared from the sampled particles. The particle size ranges used for individual particle experiments and multi-size particle experiments are summarized in Table 2. The sediment sieve size classes adopted for this research increase with a half-phi (ϕ) scale.

Table 2. Half-phi (ϕ) scale sediment sieve size ranges used for individual particle experiments (solid line) and multi-size particle experiments (dashed line) are indicated by the boxed bold lines

Phi (ϕ) Scale	Sieve Size Class Order, <i>i</i>	Retained Particle Size Range (mm)	Aggregate Name
-8 <		256 <	Boulder
-7 to -8		180-256	Large Cobble
		128-180	
-6 to -7		90-128	Small Cobble
-5 to -6	9	64-90	Very coarse gravel
	8	45-64	
	7	32-45	
-4 to -5	6	22.4-32	Coarse gravel
	5	16-22.4	
-3 to -4	4	11.2-16	Medium gravel
	3	8-11.2	
-2 to -3	2	5.6-8	Fine gravel
	1	4-5.6	
-1 to -2		2.8-4	Very fine gravel
		2-2.8	
0 to -1		1.4-2	Very coarse sand
		1-1.4	

CHAPTER III. EXPERIMENT

Two types of experiments are conducted for this research. One experiment type uses individual uniform size sediment particles for a number of experiments over a selected set of specific particle size classes, and the second is a series of experiments that include a specific design mix of particle sizes in a set of multi-size particle experiments. Each of these experiment types are described in more detail in sections 1 and 2 below.

1. Individual particle experiments – The individual particle experiments focus on single particle motion and identification of the impact characteristics of the particle on the PBIS plate. The use of a single particle size allows the variability of particle movement and impact strength to be minimized as detected by the PBIS and recorded as an impulse signal. The single particle experiments attempt to minimize the magnitude of vibrational signal interference due to sequential or simultaneous particle collisions. The PBIS impulses generated by particle impacts are indications of the average response of each channel for particles retained in a sieve size class across a range of flow discharge or hydraulic conditions. Two independent variables for this experiment are the three hydraulic conditions and up to nine retaining particle sieve size classes. The specific experimental hydraulic conditions and sieve sizes are summarized in Table 3 and were described in an earlier chapter. The detectable particle impact results in an electrical signal and is summarized as registered impulse(s) per particle in each threshold channel as a dependent variable.

For individual particle experiments, test gravels retained in sieve size classes from 4 mm to 63 mm are released individually at the sediment-feeding location upstream of the PBIS. Each test particle is fed into the flume with a time interval between consecutive test particles sufficient to eliminate vibrational signal interference. The vibration of the PBIS impact plate caused by a particle collision dissipates in less than 0.1 second in water. However, a minimum 3-second waiting time interval was employed to accommodate variability in transport velocity of individual particles and allow sufficient time for transport from the sediment-feeding location to the PBIS.

Primarily, the change of mean impulse(s) per particle in each threshold channel due to the change of two independent variables, hydraulic condition and particle retaining sieve size, can be known from the experimental results. Secondly, a detectable gravel sieve size range of each threshold channel can be determined from the variation in hydraulic conditions. Eventually a quantitative bedload estimation model for lower bedload discharge conditions, which multi-particle interaction and signal interference are negligible, can be developed based on the individual particle experiment results.

2. Multi-size particle experiments – The multi-size particle experiments simulate higher sediment discharge conditions in natural channels and stochastically measure the average responses of each channel for a 600 g equal size-fractional gravel sample. This set of experiments records signal that will include vibrational signal interference produced by multiple impacts of differently sized particles. Two independent variables for this experiment are three hydraulic conditions and three sediment-feeding rates. Average registered impulse(s) per time interval in each threshold channel is a dependent variable.

In the multi-size particle experiments a 600 g multi-size gravel sample is prepared. Hundred gram particles are sampled from each of 6 sieve size classes from 4 mm to 22.4 mm and thoroughly mixed as explained earlier in the test gravel section. A 600 g multi-size sample is released using a gravel-feeding funnel at the sediment-feeding location upstream of the PBIS. Individual experiments with three different sediment-feeding rates were conducted. The lowest average feeding rate, 20 g/s/0.2 m, is at the lower limit of signal interference effect due to multiple particle impacts. A sediment-feeding rate lower than 20 g/s/0.2 m would produce conditions similar to individual particle feeding experiments, based on preliminary results. The highest sediment-feeding rate in these experiments, 100 g/s/0.2 m, is approximately the mean mass of particles retained in the 32 mm sieve size class as explained in the test gravel section.

The multi-size particle experiments demonstrate the particle detection efficiency of the PBIS, which varies according to the degree of signal interference caused by multi-particle impacts in high bedload discharge conditions. In high sediment transport conditions, potentially higher threshold PBIS channels are triggered by constructive interference of simultaneous multi-particle impacts or multiple particle impacts over very short time interval. At the same time, the number of registered impulses may be reduced due to an increase in the duration of vibrations over a particular threshold level, masking the ability to detect a particle. Eventually a quantitative bedload estimate model considering multi-particle effects at a high sediment transport rate may be developed based on results from the multi-size particle experiments.

Table 3 summarizes both the experiment types and provides details for the sieve size classes used, the mean water discharge rate (hydraulic condition), the number of

experiments, and the particle size-fraction and sediment-feeding rate for the mixed-particle experiments.

Table 3. Experimental matrix

Experiment Type	Individual Particle	Multi-size Particle
½-φ Scale Sieve Size (mm)	4, 5.6, 8, 11.2, 16, 22.4, 32, 45, 64	4, 5.6, 8, 11.2, 16, 22.4
Size-fraction of Particle Mix	N/A	100g from each sieve size class
Average Gravel-feeding Rate (g/s)	N/A	20, 60, 100
Mean Water Discharge (m ³ /s)	0.030, 0.053, 0.076	0.030, 0.053, 0.076
No. of Experiences	More than 40 particles for each sieve size and flow discharge (> 1080 particles)	More than 10 samples for each feeding rate and flow discharge (> 90 combinations)

CHAPTER IV. RESULT

In this analysis, an electric signal “impulse” is distinguished from a physical particle “impact” because a particle impact is not always recorded by the PBIS as one impulse. An impulse is the electric signal generated by an analog voltage generator in the PBIS. Nevertheless, previous studies with a single channel type PBIS show strong correlation between the impulse signal and the quantity of bedload with long term observation data in Alpine channels (Rickenmann and Fritschi, 2010; Rickenmann and McArdell, 2007, 2008).

The mean particle registration rate is the percentage of particles in each sieve class detected at least once by the most sensitive channel 1. The mean particle registration rates obtained from individual particle experiments are plotted for the 3 experimental hydraulic conditions and by sieve size classes in Figure 12. As explained earlier, the upper limit of the test particle sieve size range is a retaining sieve size class of the largest particle which can be conveyed promptly in each experimental hydraulic condition. When the potential maximum length of the intermediate axis of a particle retained in a sieve size class is smaller than half of the control dimension, particles in the sieve size class were considered to be promptly transported. The lower limit of the test particle sieve size range is the sieve size class in which the smallest particle detected by channel 1 (most sensitive) is retained.

However, test particles passing through a 4 mm square sieve were undetected in all three experimental flow conditions. The mean particle registration rate steeply increases

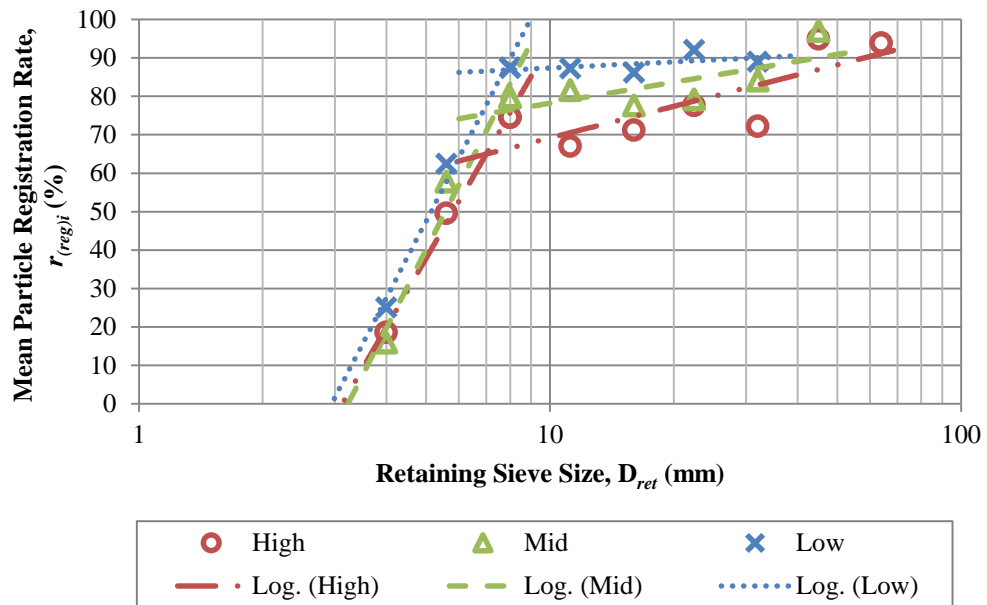


Figure 12. Comparison of mean particle registration rate by retaining sieve sizes in three different hydraulic conditions

from 0 to over 70 % between 4 mm and 8 mm sieve size classes. Particles retained in the 11.2 mm or larger sieve size classes show a 67 to 97 % mean particle registration rate. No particles in any sieve size class achieved a 100% registration rate. The tendency of mean particle registration rate in each hydraulic condition is described with two linear-log regression lines, the upper and the lower parts. The retaining sieve size range for the upper part is from 8 mm to the largest sieve size, while the lower part is from 4 mm to 8 mm sieve size class in all experimental hydraulic conditions. The lower regression lines are mathematically extrapolated. The extrapolated lower limit of detectable particle matched experiment results showing that particles passing through a 4 mm square-hole sieve were not detected. As shown, the mean particle registration rate generally increases with retaining sieve size and decreases with hydraulic condition. However, in a direct

quantitative comparison of different sieve size classes and hydraulic conditions, the trend is not valid because mean registration rates are widely scattered along the regression lines. Fluctuation of the mean registration rates, even within the same hydraulic condition, is due to two main reasons. First, non-uniform spatial sensitivity and interference from vibration signals depending on impact location across the PBIS plate (Rickenmann and Fritschi, 2010). Even though a particle makes an impact on the PBIS plate, the particle may or may not be detected due to the non-uniform spatial sensitivity of the PBIS plate. Moreover, the impulse magnitude generated from particle impact is not inversely proportional to the distance from the center of the plate. This is due to the complex and uncertain physical details of the PBIS plate geometry, and makes the intensity of vibration transmitted to the plate-centered accelerometer uncertain.

The second reason is large temporal and spatial variance of particle movement modes (e.g. hopping, rolling and sliding) (Rickenmann and Fritschi, 2010). This implies influence on particle movement by not only immeasurable temporal and spatial change of hydraulic conditions but also irregular shape and mass of particles retained in the same sieve size class. As shown in Figure 13, the study of particle motion in a Lagrangian manner helps to illustrate correlation among PBIS impulses, strength of particle impact, particle mass and hydraulic condition. The mode of particle motion and the impact strength of landing particles are determined by three forces: lift force, drag force and particle weight. Particle weight is an immutable factor and other particle forces vary according to hydraulic condition. The particle impact strength and displacement distance increases with hydraulic forces whereas probability of particle impact on the PBIS decreases with the displacement distance. The lower probability of impact at higher hydraulic condition is due to the higher

flow velocity resulting in higher drag and lift forces and longer displacement distance of particle movement. The degree of hydraulic energy transfer to particles also depends on the physical properties of a given particle, such as mass and shape.

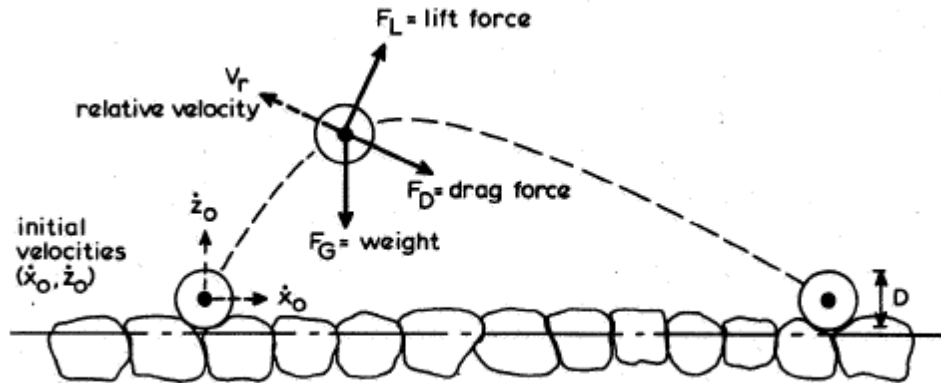


Figure 13. Definition sketch of particle saltation (Rijn, 1984)

The individual particle experiment results are summarized in Table 4 and the mean impulse per particle in four different threshold channels are plotted in Figure 14 (a)-(c), by hydraulic condition. The mean impulses per particle in 8 mm and larger sieve size classes are higher than one in channel 1 for all three hydraulic conditions and increase up to 2.5 depending on particle sieve size and hydraulic condition. More than one impulse per particle on average might infer particles larger than 8 mm are usually transported in the particle movement mode which has shorter displacement distance than a longitudinal dimension of the PBIS plate such as rolling or sliding. The shorter mean displacement distance increases the probability of multiple impacts on the PBIS plate and results in multiple impulse signals generated in lower threshold channels. Yet the particle size may not be significant enough for the impact energy to register an impact for the higher

threshold channels. In consideration of this behavior, the mean registration rates are almost 70-90 % in channel 1 in Figure 12, and it can be speculated from individual experiment results that particles retained in 8mm sieve size class frequently cause more than one impact.

Particles passing through an 11.2 mm sieve size class are not detected by channel 2 which has a higher threshold than channel 1. Unlike in channel 1, the mean impulse per particle in channel 2 is not partially declined or flattened with the increment of test particle sieve size class and experimental hydraulic condition, although it increases up to 1.6 impulses per particle in high hydraulic conditions. Thus, the mean impulses per particle in channel 2 are well-correlated with particle sieve size class and have R-square values higher than 0.92 for all hydraulic conditions.

Although not shown in Figure 14, the mean number of impulses per particle, for sizes larger than the upper limit sieve size, increased up to 3 for channel 1 in low hydraulic conditions and flattened out in channel 2. Moreover, particles larger than the upper limit sieve size in each hydraulic condition caused significant change of hydraulic condition while being conveyed downstream. This explains why the upper sieve size limits of test particle vary by hydraulic condition.

The mean impulses per particle in each channel generally vary in direct proportion to the particle sieve size class increment and tend to vary inversely proportional with hydraulic force increment as shown in Figure 14. However, the mean impulse per particle does not directly indicate the particle impact magnitude or particle size. The mean impulse per particle in each channel is dominantly influenced by the likely modes of bedload

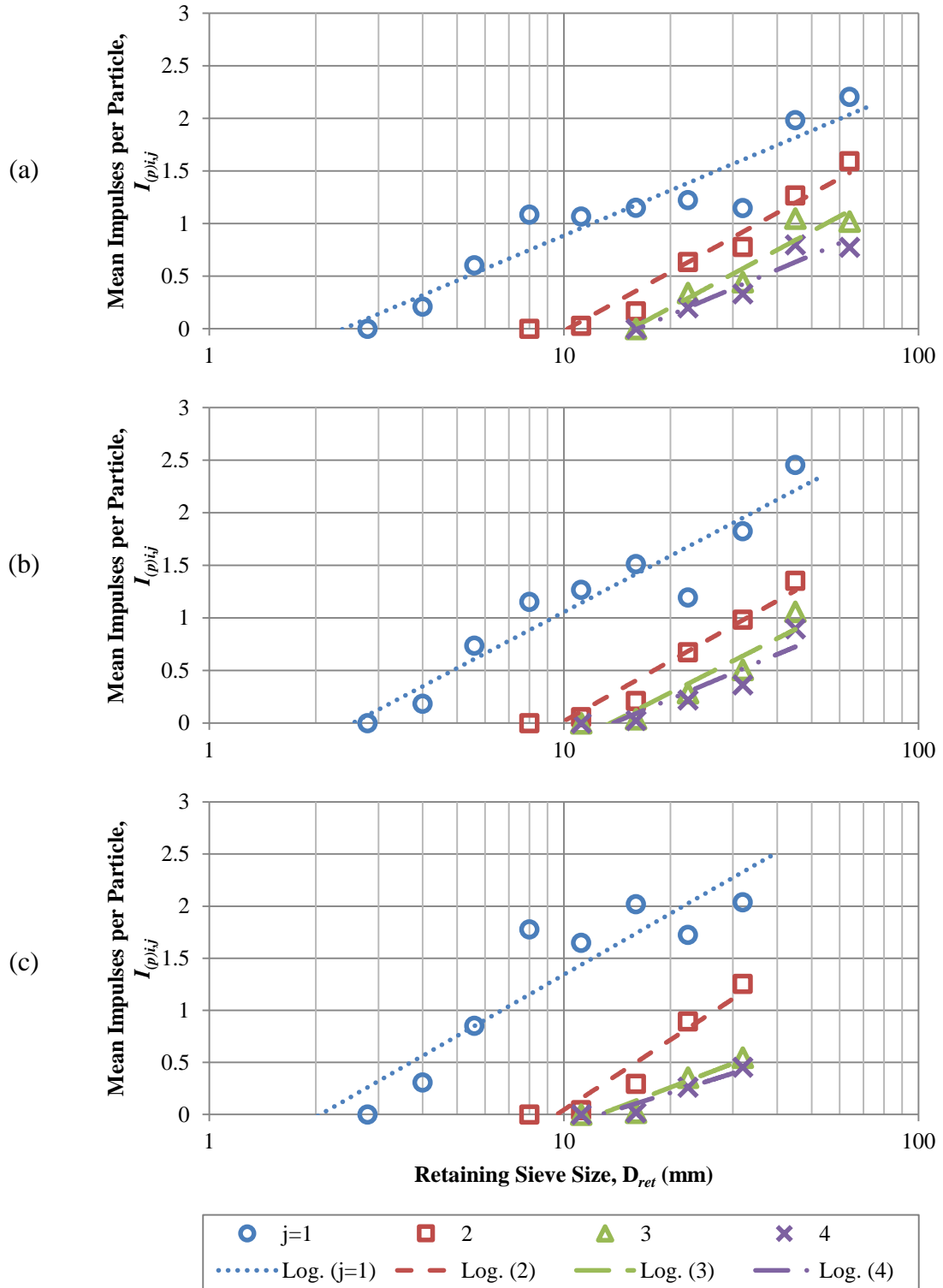


Figure 14. Mean impulses by particle retaining sieve size class in three different hydraulic condition (Bed shear stress = (a) 38.0 Pa, (b) 28.7 Pa and (c) 19.5 Pa)

Table 4. Summary of the individual particle experiment results

Mean Bed Shear Stress, τ (Pa)	Particle Sieve Size Class Order, i	Retaining Particle Sieve Size, D_{ret} (mm)	*Mean Particle Mass, $m_{(p)i}$ (g)	No. of Test Particles, $N_{(p)i}$	No. of Registered Particles, $N_{(reg)i}$	**Particle Registration Rate, $r_{(reg)i}$ (%)	Total No. of Impulses, $I_{i,j}$				***Mean Impulses per Particle, $I_{(p)i,j}$			
							$j = 1$ (Ch1)	2 (Ch2)	3 (Ch3)	4 (Ch4)	$j = 1$	2	3	4
19.5	1	4	0.2	183	46	25	56				0.31			
	2	5.6	0.5	224	140	63	191				0.85			
	3	8	1.4	80	70	88	141				1.78	0		
	4	11.2	4.1	71	62	87	117	3			1.65	0.04	0	0
	5	16	12.4	58	50	86	117	17	1	1	2.02	0.29	0.02	0.02
	6	22.4	35.6	76	70	95	131	68	27	20	1.72	0.89	0.36	0.26
	7	32	108.9	55	49	89	112	69	30	25	2.04	1.25	0.55	0.45
28.7	1	4	0.2	194	31	16	36				0.19			
	2	5.6	0.5	140	81	58	103				0.74			
	3	8	1.4	79	63	80	91				1.15	0		
	4	11.2	4.1	71	58	82	90	4			1.27	0.06	0	0
	5	16	12.4	76	59	78	115	16	3	2	1.51	0.21	0.04	0.03
	6	22.4	35.6	77	61	83	92	52	22	17	1.19	0.68	0.29	0.22
	7	32	108.9	63	53	84	115	62	32	23	1.83	0.98	0.51	0.37
	8	45	316.8	68	66	86	167	92	72	61	2.46	1.35	1.06	0.90
38.0	1	4	0.2	209	39	19	44				0.21			
	2	5.6	0.5	121	60	50	73				0.60			
	3	8	1.4	165	123	75	179				1.08	0		
	4	11.2	4.1	73	49	67	78	2			1.07	0.03		
	5	16	12.4	66	47	71	76	11	2	1	1.15	0.17	0	0
	6	22.4	35.6	85	66	76	104	54	29	17	1.22	0.64	0.34	0.20
	7	32	108.9	54	39	72	62	42	24	18	1.15	0.78	0.44	0.33
	8	45	316.8	60	57	81	119	76	63	48	1.98	1.27	1.05	0.80
	9	64	908.8	49	46	91	108	78	50	38	2.20	1.59	1.02	0.78

*Mean particle mass, $m_{(p)i}$, is calculated using the particle size and mass correlation equation for Harrison Fork in Figure 11.

**Particle registration rate, $r_{(reg)i}$ (%) = $\frac{\text{The Number of registered particles in the lowest threshold channel 1, } N_{(reg)i}}{\text{The number of test particles, } N_{(p)i}} \times 100(\%)$

***Mean impulses per particle, $I_{(p)i,j}$ = $\frac{\text{The number of impulse in each channel, } I_{i,j}}{\text{The number of test particles, } N_{(p)i}}$

particle motion. The mean impulse per particle is an arithmetic mean of the number of impulses generated by test particles for a single sieve size class and a certain hydraulic condition. The mean impulses per particle reflect probabilistic performance of the PBIS according to particle size in a given hydraulic condition based on the law of large numbers (LLN). The point values in Figure 14 do not indicate the universal absolute quantity of bedload because they imply the probabilistic performance of the PBIS influenced by all factors mentioned above.

As an example, 32 mm particles are potentially heavy enough to trigger the highest threshold channel 4 when they make an impact on the center of the PBIS plate, as was demonstrated in an underwater particle drop test from a 300 mm height. However, the mean impulse per particle for the 32 mm sieve size class is below 1 in channel 4 for all hydraulic conditions. The mean impulse per particle for the 32 mm sieve size class in channel 1 decreases from approximately 2 to 1 and decreases from approximately 0.5 to 0.3 on channel 4 with an increment change of hydraulic energy. Moreover, the mean impulses per particle for the 32 mm sieve size class in channel 1 is very similar to what particles in the 8 mm sieve size class generate, on average, in low and high hydraulic conditions. Considering that the mean registration rate of 32 mm particles in high hydraulic conditions is almost 10 % lower than in other hydraulic conditions. This can be interpreted to imply the mean impulses per particle for the 32 mm sieve size class in channel 4 decreases due to the rate of particle misses in high hydraulic conditions rather than the decline of the impact force. It might also be due to the likely mode of particle motion changes with changing hydraulic conditions, such as change from sliding to hopping. Specifically, the particle displacement distance increases on average with increase in hydraulic condition.

The decline of mean impulses per particle for the 32 mm sieve size class is more than the increment of the particle missing rate in lower threshold channels 1 and 2. The result verifies that hydraulic effects on the modes of particle motion predominantly affect the probabilistic performance of the PBIS. Therefore, these experimental results can be applied to limited conditions but are insufficient to interpret hydraulic boundary conditions for particle motion modes for any particle size class. The PBIS must be implemented and a site-specific calibration performed prior to use for any investigation of channel bedload.

Based on the mean impulses per particle determined from individual particle experiment results, the mean impulses for a 600g equal size-fraction gravel sample was estimated. The 600g gravel samples were used in a series of multi-size particle experiments and the mean impulses were determined from the data recorded by each threshold channel. The results of these estimations are summarized in Table 5 for the three hydraulic conditions. Herein predicted mean impulse per sample implies mean impulse directly estimated according to the individual particle experiment results. Thus, change of mean impulse by multi-particle effects are not considered on the predicted impulse values. On the contrary, mean impulse from the multi-size particle experiments is called as estimated mean impulse. As explained in the experiment set-up, half-phi (ϕ) scale sieve classes from 4 mm to 22.4 mm were selected to create 600 g equal size-fraction gravel sample and the mean particle mass in the sieve classes is less than 100 g per particle. Using the particle size and mass correlation equations developed for test gravel in Figure 11, the mean number of particles per 100 g gravel sample in each sieve class is defined. The predicted mean impulses per 600 g equal size-fraction gravel samples are the sum of the predicted impulses per each 100 g particles in the six sieve classes. The predicted mean impulse

values can be expected unless there is interaction among bedload particles and signal interference due to vibration caused by other particles, with the exception of a particle itself. Additionally, the particle sample size in each sieve class must be large enough to meet the conditions of LLN.

Four charts in Figure 15 (a)-(d) are a graphical comparison of the predicted impulses based on the individual particle experiments with the estimated impulses based on observations from the multi-size particle experiments. The estimated and predicted impulses are summarized in Table 6. To compare the probabilistic performance of the PBIS according to change of bedload transport rate, three different gravel sample feeding rates were used for the multi-size particle experiment. As explained in the experiment set-up, in order to simulate three different bedload transport rates, the 600 g equal size-fraction gravel samples are released over three time durations: 30 seconds (1200 g/min/0.2 m), 12 seconds (3000 g/min/0.2 m), and 6 seconds (6000 g/min/0.2 m). The three sediment-feeding rates are applied in the three hydraulic conditions, as in the individual particle experiments. The multi-size particle experiment results for equally sized gravel

Table 5. Predicted impulses for 600g multi-size gravel sample according to the individual particle experiment

Mean Bed Shear Stress, τ (Pa)	Particle Sieve Size Class Order, i	Retaining Particle Sieve Size, D_{ret} (mm)	*Mean Particle Mass, $m_{(p)i}$ (g)	*Mean No. of Particles per 100g, $N_{(100)i}$	**Mean Impulse per Particle from Individual Particle Experiment, $I_{(p)i,j}$				***Predicted Mean Impulses per 100g Particles in Each Sieve Class, $P_{(100)i,j}$				†Predicted Mean Impulses for 600g Equal Size-fraction Gravel Sample, $P_{(600)1-6,j}$			
					$j = 1$ (Ch1)	2 (Ch2)	3 (Ch3)	4 (Ch4)	$j = 1$	2	3	4	$j = 1$	2	3	4
19.5	1	4	0.16	619	0.3				189.5				560.6	5.9	1.1	0.9
	2	5.6	0.46	216	0.9				184.1							
	3	8	1.42	71	1.8				125.4							
	4	11.2	4.06	25	1.6				40.6	1.0						
	5	16	12.42	8	2.0	0.3			16.2	2.4	0.1	0.1				
	6	22.4	35.62	3	1.7	0.9	0.4	0.3	4.8	2.5	1.0	0.7				
28.7	1	4	0.16	619	0.2				114.9				401.8	5.0	1.1	0.6
	2	5.6	0.46	216	0.7				158.8							
	3	8	1.42	71	1.2				81.3							
	4	11.2	4.06	25	1.3	0.1			31.2	1.4						
	5	16	12.42	8	1.5	0.2			12.2	1.7	0.3					
	6	22.4	35.62	3	1.2	0.7	0.3	0.2	3.4	1.9	0.8	0.6				
38.0	1	4	0.16	619	0.2				130.4				376.2	3.8	1.0	0.6
	2	5.6	0.46	216	0.6				130.2							
	3	8	1.42	71	1.1				76.6							
	4	11.2	4.06	25	1.1				26.3	0.7						
	5	16	12.42	8	1.2	0.2			9.3	1.3						
	6	22.4	35.62	3	1.2	0.6	0.3	0.2	3.4	1.8	1.0	0.6				

*Mean number of particles per 100g in a sieve size class i , $N_{(100)i} = \frac{100 (g)}{\text{Mean particle mass in a sieve size class } i, m_{(p)i} (g)}$

**Mean impulse per particle, $I_{(p)i,j}$, is from the summary of the individual particle experiment results in Table 4.

***Predicted mean impulses per 100g particles in a sieve size class i , $P_{(100)i,j} = \text{Mean number of particles per 100g, } N_{(100)i} \times \text{Mean impulse per particle, } I_{(p)i,j}$

†Predicted mean impulses for 600g equal size-fraction sample, $P_{(600)1-6,j} = \sum_{i=1}^6 \text{Predicted mean impulses per 100g particles in a sieve size class } i$

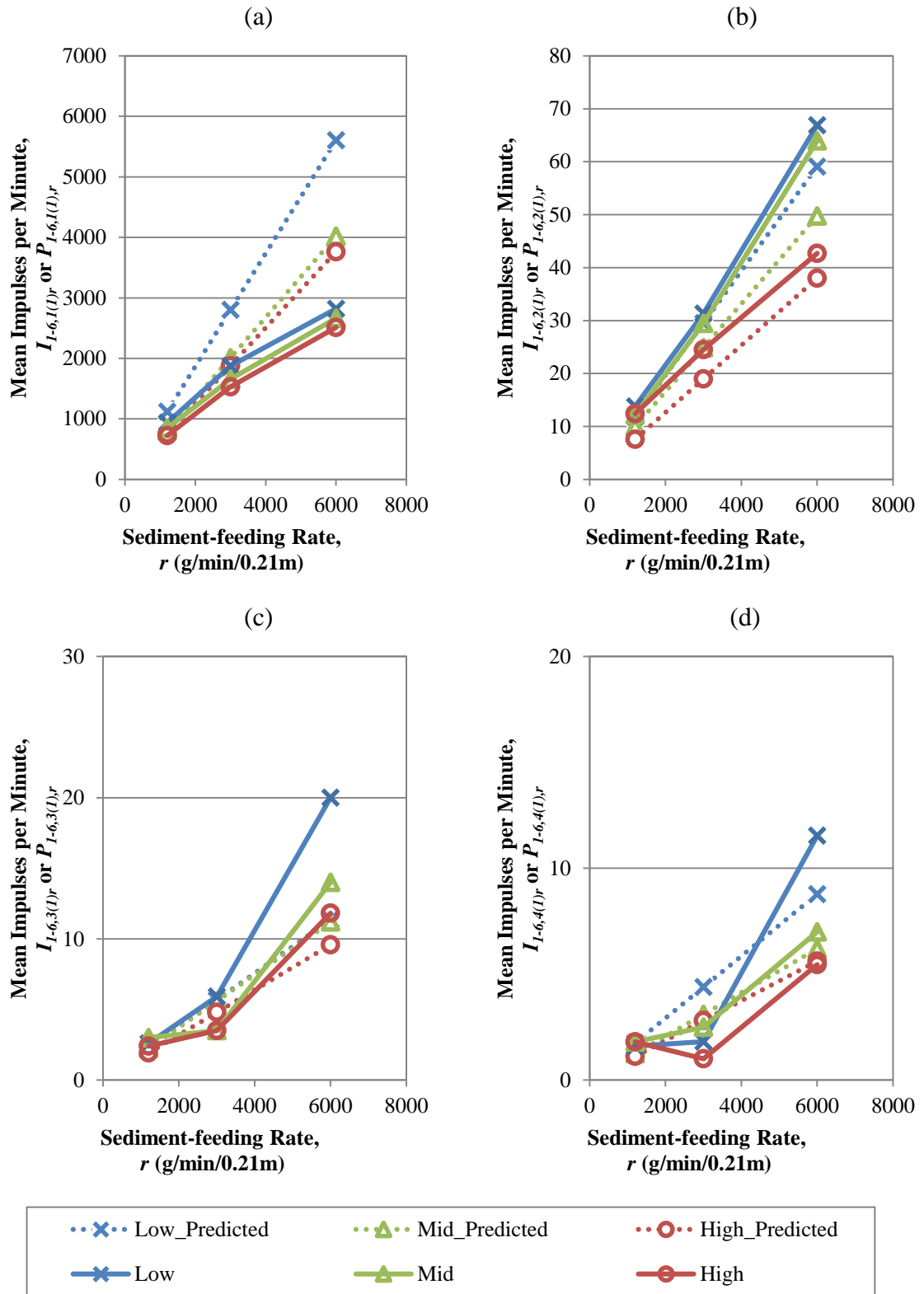


Figure 15. Comparison between the predicted and the estimated mean impulses per minute for equal size-fraction gravel sample in each channel
 ((a) $j = 1$, (b) 2, (c) 3 and (d) 4)

samples in nine conditions are converted to the estimated impulses in a one-minute sampling period. Therefore, the estimated mean impulses per minute in nine bedload transport scenarios are based on observed values of the multi-size particle experiments. The multi-particle experiment results are shown as solid lines in Figure 15. Predicted mean impulses per minute calculated using the mean impulses per particle from the individual particle results are shown as dashed lines.

The minimum time width of a digital pulse is about 0.004 seconds. The ideal number of maximum impulses that can be recorded by the PBIS for a 60-second sampling interval is about 15,000 and the mean number of particles released for 60 seconds with 100g/s/0.2 m sediment-feeding rate and the same particle size-fraction as the multi-size experimental gravel sample is 9,420. Therefore, the theoretical capacity of the PBIS is sufficient to detect every particle impact during the experiment. Additionally, all particles in a 6 kg equal size-fraction gravel sample are ideally distributed for 60 seconds and would generate single isolated impacts and impulse signals one by one. However, a notable reduction of impulses during the multi-particle experiments begins at approximately 700 impulses per minute in the lowest threshold channel 1, as shown in Figure 15 (a), although the degrees of impulse reduction vary depending on hydraulic condition and mean designed sediment-feeding rate. Data indicate the number of impulses decreases in proportion as the number of detectable particles increases in a given sampling interval due to multi-particle effects.

In the lowest threshold channel 1, the highest estimated mean impulses per minute are only 2,823 in the lowest hydraulic condition with the highest feeding rate. For all nine experimental conditions, the estimated mean impulses per minute are less than

Table 6. Summary of the multi-size particle experiment results and comparison with the predicted mean impulses calculated based on the individual particle experiment results

Mean Bed Shear Stress, τ (Pa)	Mean Designed Sediment-feeding Rate, Q_{s-feed} (g/s/0.2 m)	Mean Sediment-feeding Duration, t_{s-feed} (sec/600g)	Mean Impulses per 600g Multi-size Particle Sample, $I_{(600)1-6,j,r}$ or $*P_{(600)1-6,j}$				**Estimated Mean Impulses per Minute w/ Designed Sediment-feeding Rate, $I_{1-6,j(1),r}$				***Predicted Mean Impulses per Minute Based on Individual Particle Experiment, $P_{1-6,j(1),r}$			
			$j = 1$ (Ch1)	2 (Ch2)	3 (Ch3)	4 (Ch4)	$j = 1$	2	3	4	$j = 1$	2	3	4
19.5	20	30	468.1	6.9	1.3	0.8	936.2	13.8	2.6	1.6	1121	12	2	2
	50	12	375.4	6.3	1.2	0.4	1876.8	31.4	5.9	1.8	2803	30	6	4
	100	6	282.3	6.7	2.0	1.2	2823.1	66.9	20.0	11.5	5606	59	11	9
	Individual Particle			560.6	5.9	1.1	0.9	N/A						
28.7	20	30	424.3	6.1	1.5	0.9	848.6	12.2	3.0	1.8	804	10	2	2
	50	12	331.3	5.9	0.7	0.5	1656.5	29.5	3.5	2.5	2009	25	6	3
	100	6	266.4	6.4	1.4	0.7	2664.0	64.0	14.0	7.0	4018	50	11	6
	Individual Particle			401.8	5.0	1.1	0.6	N/A						
38.0	20	30	361.5	6.2	1.2	0.9	723.0	12.4	2.4	1.8	752	8	2	1
	50	12	306.6	4.9	0.7	0.2	1533.0	24.5	3.5	1.0	1881	19	5	3
	100	6	251.4	4.3	1.2	0.5	2513.6	42.7	11.8	5.5	3762	38	10	6
	Individual Particle			376.2	3.8	1.0	0.6	N/A						

*Predicted mean impulses per 600g multi-size particle sample, $P_{(600)1-6,j}$, is the prediction based on the individual particle experiment in Table 5.

**Estimated mean impulses per minute, $I_{1-6,j(1),r} = \frac{60 \text{ (sec/min)}}{\text{Sediment-feeding Duration, } t_{s-feed} \text{ (sec/600g)}} \times$

Estimated mean impulses per 600g mixed size particle sample, $I_{(600)1-6,j}$

***Predicted mean impulses per minute, $P_{1-6,j(1),r} = \frac{60 \text{ (sec/min)}}{\text{Sediment-feeding Duration (sec/600g)}} \times$

Predicted mean impulses per 600g individual particles from six sieve classes, $P_{(600)1-6,j}$

the predicted mean impulses per minute. Moreover, as shown in Figure 15 (a), the estimated mean impulses per minute for each sediment-feeding rate are closely spaced, regardless the experimental hydraulic condition. The largest difference in the estimated mean impulses per minute for each sediment-feeding rate is 344, with 50 g/s/0.2 m, between low and high hydraulic conditions. That is 22 % of the lowest mean impulse, $I_{6,1(1),3000} = 1533$, whereas the largest difference in the predicted mean impulses per minute for each sediment-feeding rate is 49 %. The bias between predicted and estimated mean impulses per minute increases non-linearly with the mean sediment-feeding rate due to particle interaction and impact signal interference in multi-size particle experiments. The degree of bias in the 100 g/s/0.2 m sediment-feeding rate in low experimental hydraulic conditions is much larger than in the other two hydraulic conditions, and the predicted mean impulses per minute is approximately 100 % more than the estimated mean impulses per minute.

While the predicted mean impulses per minute are overestimated in channel 1, they are underestimated in channel 2 for all experimental conditions. The estimated mean impulses per minute show a similar linearly proportional tendency with the predicted mean impulses per minute as shown in Figure 15 (b). The largest bias between predicted and estimated mean impulses per minute for each sediment-feeding rate is only -15 % in mid-hydraulic conditions with a 100 g/s/0.2 m sediment-feeding rate. The predicted mean impulses per minute which are higher than the estimated mean impulses per minute in channel 2 might be due to impact signal contribution of multi-particles, since single particles alone cannot trigger channel 2 with a sufficient time gap.

The smallest particle sieve size class which can trigger channels 3 and 4 in the individual particle experiments is 22.4 mm. The mean impulses per particle for the 22.4 mm sieve size class in channels 3 and 4 are 0.4 and 0.3 in low hydraulic conditions, as shown in Table 5. The mean number of particles in the 22.4 mm and 16 mm sieve size classes which may trigger channels 3 and 4 number only 11 in a 600 g equal size-fraction gravel sample. Considering that the damping period from impact to rest state of the PBIS plate caused by 22.4 mm particles is always less than 0.02 seconds in water, the probability of these 11 particles causing impacts within a 0.02 second or less time window, and then recorded as one impulse, is very low. Without considering the area of the PBIS plate and the mode of particle motion, the probability that two of the 11 particles impact in less than a 0.02 second time interval is less than 0.1 % with the 100 g/s/0.2 m sediment-feeding rate and less than 0.03 % with other feeding rates.

CHAPTER V. ANALYSIS

The data from the multi-channel PBIS are the number of impulses recorded for a sampling time interval by four threshold channels. This is similar to the data produced by other indirect bedload measurement methods, where the data do not directly indicate either the number or size of particles. Thus, a calibration process is required to quantify the mass of bedload and estimate the particle-size distribution.

In this study, results indicate that, hydraulic condition affects the mode of bedload particle motion during individual particle experiments. In the multi-size particle experiments, results indicate multi-particle interaction on the mode of bedload particle motion and signal interference from consecutive multi-particle impacts.

According to both types of experiments, single- and multi-particle, the mean number of impulses in each threshold channel is influenced by hydraulic condition, particle sieve size, and designed sediment-feeding rate. In this analysis, mean bed shear stress (BSS) represents experimental hydraulic conditions. The standard time interval for the analysis is one minute which is considered a long enough period to satisfy the condition of the law of large number (LNN) and a short enough period to realize the changing pattern of bedload transport.

All three independent variables, hydraulic condition, particle sieve size class, and designed sediment-feeding rate, have a range of variance and can be expressed as a function of parameters such as Reynolds number, particle angularity and particle travel time. These

parameters are implicitly part of the experiment data and indicate high degrees of freedom in characterizing the overall bedload transport mechanism. Nevertheless, an analysis was conducted with mean values of variables in an Eulerian manner by looking at the pulsatile bedload particle transport through a cross-section of channel as a sediment concentration in a unit volume of water flowing through the cross-section of channel in a certain sampling time. This means the assumption that independent and dependent variables of the experiments are normally distributed with small variance and the sample size of variables is large enough to satisfy the LLN. The analysis implies a probabilistic correlation between the actual bedload and the impulse response. Under this assumption, the experiment-derived analytical results allow development of a bedload estimate model.

The correlation between sieve size and the mean mass of particles retained in the sieve is shown in Figure 11 and presented in an inversed form in Figure 16. Figure 16 shows the number of particles per unit mass (= 1 g). In other words, the y-variable in Figure 16 is a reciprocal of the y-variable in Figure 11. By assuming a particle produces an impulse in the PBIS, the number of particles per unit mass in Figure 16 is the number of impulses per unit mass (= 1 g). Thus, the linear-log regression line in Figure 16 defines the ideal mean impulse line. This implies one impulse per particle in the selected particle sieve size class. For example, the mean mass of particles retained in the 8 mm sieve size class is approximately equivalent to one particle per gram.

The solid straight line in Figure 17 is the ideal mean impulse line from equation (1) and Figure 16. Experiment data are compared with the ideal impulse line in Figure 17 for individual particle experiments. Experiment data is averaged and values on the right side of the ideal impulse line indicate particles generating more than one impulse, whereas

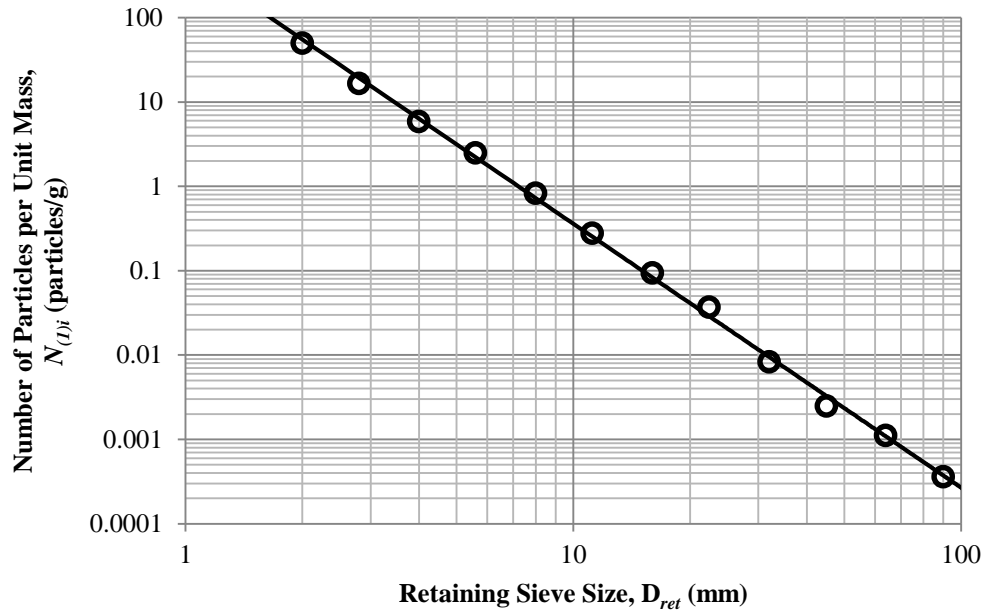


Figure 16. Mean number of particles per unit mass (= 1 g) for retaining sieve sizes

points on the left side of the ideal impulse line indicate a mean impulse per particle less than one. The vertical dash line shows the particle size associated with a one-impulse per particle in the mid-hydraulic experimental condition. In the lowest threshold, channel 1 in Figure 17 (a), particles smaller than the 8 mm sieve size were found to generate less than one impulse per particle. In each channel 2 and 3 in Figure 17 (b) and (c), the mean impulses of particles smaller than the 32 mm and 45 mm sieve size each are less than one per particle. The mean impulses are below one per particle in channel 4 over the entire experimental particle size range.

$$\begin{aligned}
 & \text{Mean impulse per unit mass in a sieve size class } i, I_{(1)i,j} \text{ (impulses/g)} & (1) \\
 & = \frac{\text{Mean impulse per particle in a sieve size class } i, I_{(p)i,j} \text{ (impulses/particle)}}{\text{Mean particle mass in a sieve class } i, m_{(p)i} \text{ (g/particle)}}
 \end{aligned}$$

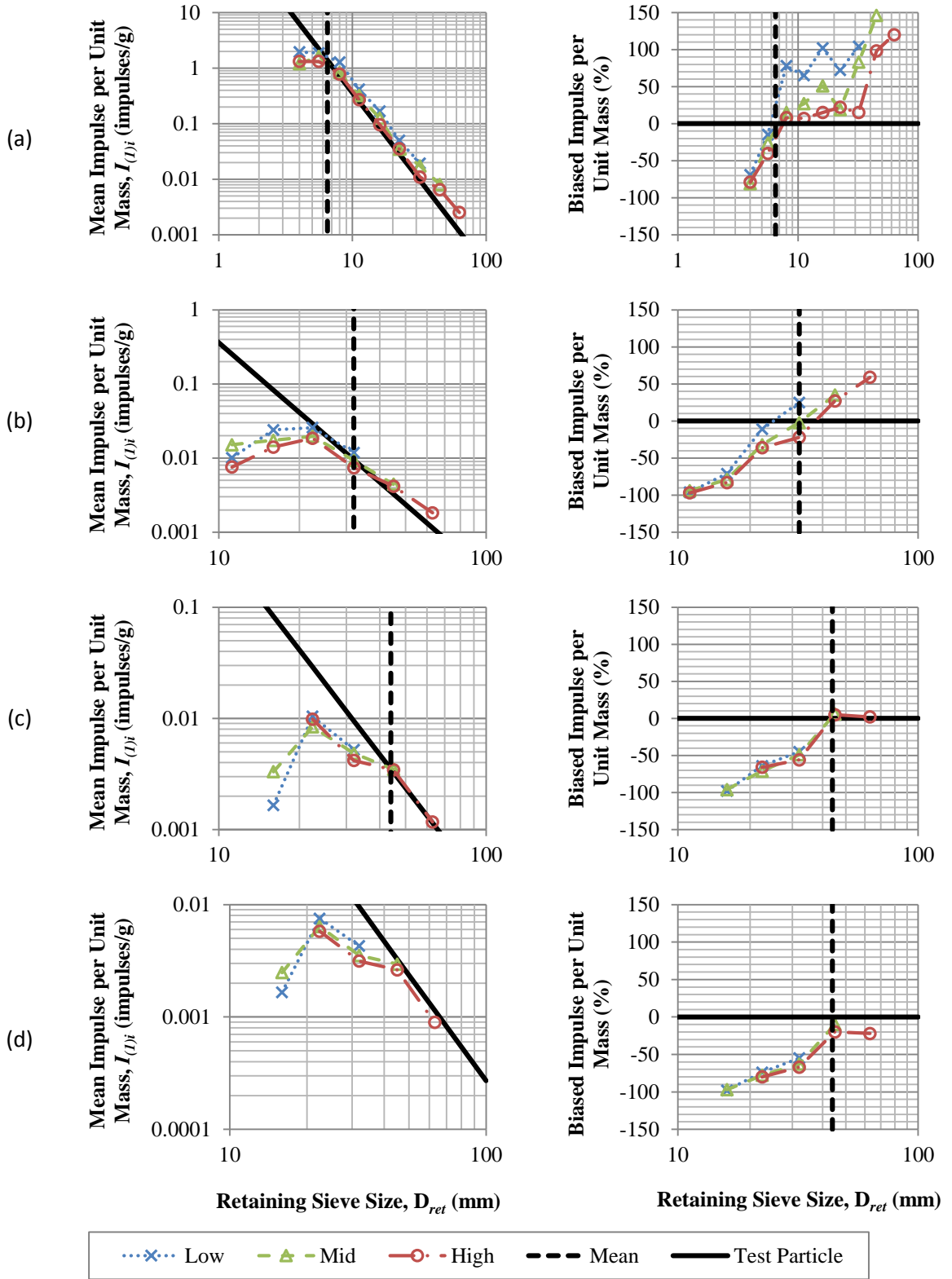


Figure 17. Comparison between the mean impulses per 1 g unit mass and one impulse per particle line in each channel ((a) $j = 1$, (b) 2, (c) 3 and (d) 4)

The bias in the mean impulses per unit mass (= estimated) from the ideal mean impulse (= expected) line is displayed in Figure 17 on the right-side plots. The bias is the difference between the expected and the estimated values and this difference is divided by the expected value. The bias is less than $\pm 150\%$ in all four threshold channels and follows a similar pattern regardless of hydraulic conditions except in channel 1. The bias in channel 1 depends on particle sieve size and hydraulic conditions. This is an indication of the bias associated with a single channel PBIS. If the bias of the mean impulses per unit mass is at or below $\pm 150\%$, none or a constant adjustment coefficient might be sufficient to achieve similar or better accuracy of quantitative bedload estimate from a single channel PBIS than any estimates based on bedload transport formulas.

The charts on the left-side in Figure 17 are reconstructed in Figure 18 as the dimensionless impulse frequency ratio of each particle sieve size for an equal size-fraction gravel sample composed of transportable particles in each hydraulic condition. The relative and cumulative mean impulse frequency distributions are plotted in Figure 18 (a)-(d) by each threshold channel ($j = 1, 2, 3$ and 4). The relative mean impulse frequencies, $f_{i,j}$, are from equation (2) and shown as dash lines. The relative mean impulse frequency is the ratio of the mean impulses caused by particles in sieve size class i to the total impulses caused by an equal size-fraction between $i = 1$ and the largest particle size class (max) used in the individual particle experiment. Thus, the largest particle size class, max, is a variable set by the hydraulic condition. The cumulative mean impulse frequencies, $F_{(1-n),j}$, are from equation (3) and shown as solid lines in Figure 18. The cumulative mean impulse frequency, $F_{(1-n),j}$, is the integration of the relative mean impulse frequencies in the retaining sieve size classes, from $i = 1$ to n .

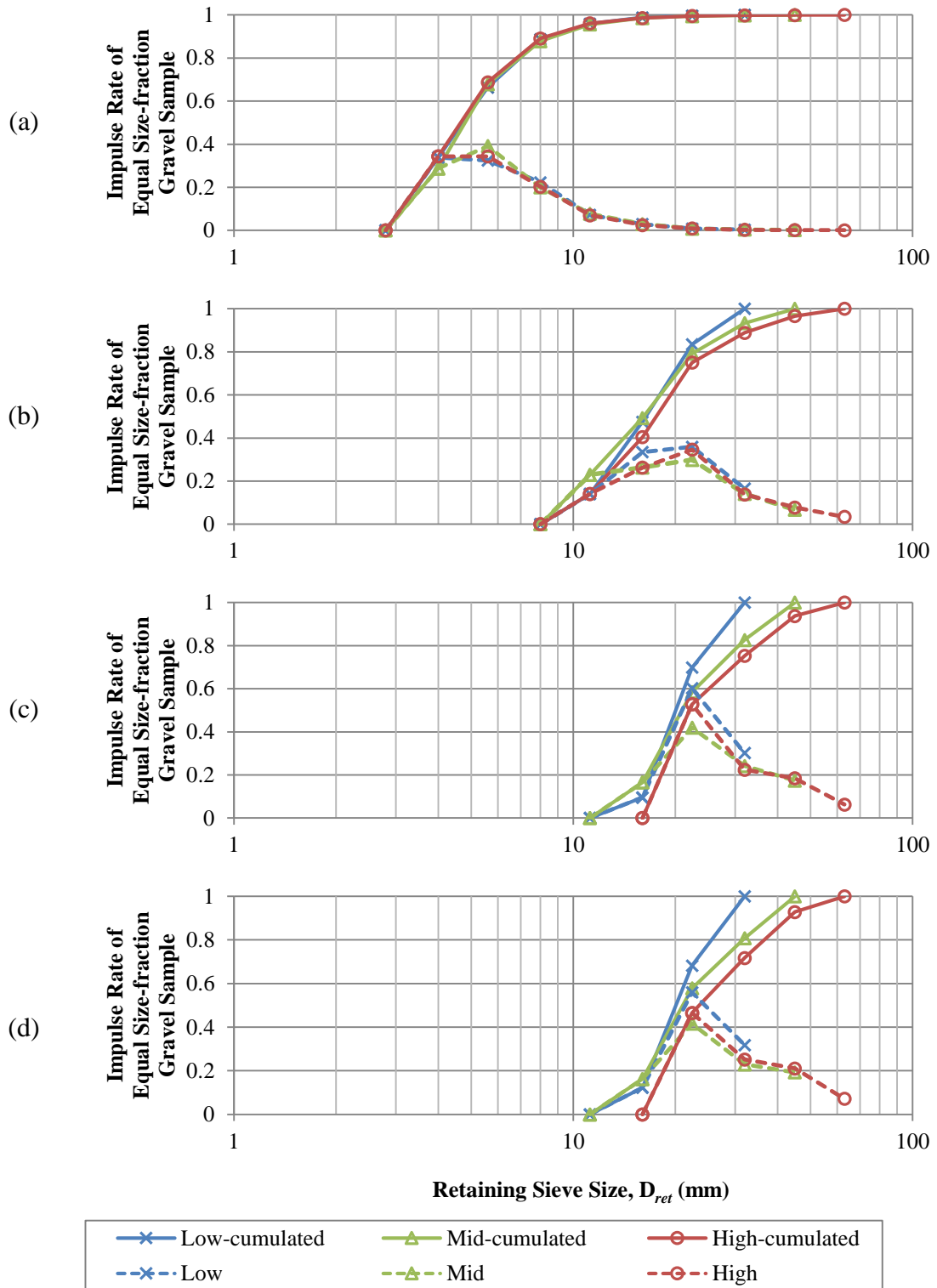


Figure 18. Cumulative and relative mean impulse frequency distribution of equal size-fraction gravel sample in each channel ((a) $j = 1$, (b) 2, (c) 3 and (d) 4)

$$\begin{aligned} & \text{Relative mean impulse frequency, } f_{i,j} & (2) \\ & = \frac{\text{Mean impulse per unit mass in a sieve size class } i, I_{(1)i,j} \text{ (impulses/g)}}{\sum_{i=1}^{max} \text{Mean impulse per unit mass in a sieve size class } i, I_{(1)i,j} \text{ (impulses/g)}} \end{aligned}$$

$$\begin{aligned} & \text{Cumulative mean impulse frequency, } F_{(1-n),j} & (3) \\ & = \sum_{i=1}^n \text{Relative mean impulse frequency, } f_{i,j} \\ & = \frac{\sum_{i=1}^n \text{Mean impulse per unit mass in a sieve size class } i, I_{(1)i,j} \text{ (impulses/g)}}{\sum_{i=1}^{max} \text{Mean impulse per unit mass in a sieve size class } i, I_{(1)i,j} \text{ (impulses/g)}} \end{aligned}$$

In channel 1, approximately 90% of total impulses are generated by particles passing through the 11.2 mm sieve. Then, impulses caused by larger particles retained in the 11.2 mm sieve are negligible. In other words, impulses in channel 1 by particles passing through the 11.2 mm sieve size class are considerably unaffected by particles retained in the 11.2 mm sieve. The total impulses registered in channel 1 can be considered to represent the quantity of particles passing through the 11.2 mm sieve. Therefore, implied particle size boundaries of channel 1 are as summarized in Table 7. This means the experimental hydraulic conditions provide adequate force to convey larger gravels beyond the upper particle sieve size boundary of channel 1.

In the same way, approximately 90% of total impulses registered in channel 2 are generated by particles retained in sieve size classes between 11.2 mm and 32 mm. However, the cumulative mean impulse frequency distributions for channel 2 do not show a similar level of convergence. In order that the cumulative frequency distribution of channel 2

Table 7. Upper and lower boundaries of represented sieve size classes of each channel in three experimental hydraulic conditions

	$j = 1$	2	3	4
Lower Boundary Sieve Size, D_{jrl} (mm)	4	11.2	~16	~16
Upper Boundary Sieve Size, D_{jru} (mm)	8	~32	Undetermined	Undetermined

reaches convergence, an experiment with a wider range of particle sizes and higher hydraulic condition is required. This would provide higher energy to convey particles retained in a 90 mm sieve size class. Nevertheless, practicability in bedload estimate analysis can override the meaning of statistical convergence based on these experimental results. In this study, the relative mean impulse frequency of particles retained in the 45 mm sieve size class is less than 0.05 in the high flow hydraulic condition. That indicates experimental results are sufficient to determine the particle size boundaries of channel 2 since the likelihood of transport of particles larger than 63 mm sieve size class in hydraulic conditions comparable to the high experimental hydraulic condition is extremely low in nature. Considering a mean particle in the 90 mm sieve size class transported within an equal particle size-fraction in a one-minute sampling interval, the mean bedload transport rate detected by the PBIS is over 400 g/s. The 400 g/s gravel transport rate in a 38 Pa bed shear stress condition is rare in nature. Moreover, a case which a 90 mm size particle is transported in a one minute sampling interval is extremely rare in the same hydraulic condition. Thus, the mean impulses per a unit mass for particles retained in the 90 mm sieve size class is too low to influence the relative mean impulse frequency of channel 2. Therefore, in terms of practicability in bedload estimate, it can be determined that the cumulative mean impulse frequency distribution in channel 2 converges into 100 % in the

45 mm and larger particle sieve size classes. In addition, impulses caused by particles passing through the 11.2 mm or retained in the 45 mm sieve size class in the three experimental hydraulic conditions are considered negligible in channel 2 data.

The cumulative mean impulse frequency distributions for channels 3 and 4 do not reach a level of convergence in the experimental conditions as shown in Figure 18 (c) and (d). This is due to the experimental particle sizes selected for in use were not representative of the size classes detected by channels 3 and 4. Moreover, the analytical assumptions, that a large enough number of particles and equal particle size-fraction for a sampling interval, cannot be satisfied at a transport rate below 100 g/s/0.2 m with particles retained in 45 mm or larger sieve size classes. Therefore, the upper limit on sieve size boundaries for channels 3 and 4 are undetermined in Table 7.

According to the comparison of mean impulse frequency distributions, equation (4) is proposed to estimate the transport rate of bedload in gram per sampling interval. The bedload estimate equation has a linear form that multiplies impulses registered in each channel, I_j , by a calibration coefficient, c_j . The calibration coefficients in equation (4) are reciprocals of the arithmetic mean of the number of impulses per unit mass, $I_{(1)i,j}$, for particles which are retained in the sieve size classes of channel j as shown in equation (5). The calibration coefficients are variable by BSS as shown in Table 8 and thus can be expressed as functions of BSS and represented by the linear regression equations in Figure 19. The estimation error in fitting equation (4) to experiment data is mainly due to differences between the detectable and representative sieve size class of channel j . Even though the mean impulses by BSS were reflected in the calibration coefficients, equation

(4) is applicable only for low bedload transport rate conditions since multi-particle effects observed in the multi-size particle experiments are negligible.

$$Q_{s-estimate} = c_1 I_1 + c_2 I_2 + c_3 I_3 + c_4 I_4 - \varepsilon \quad (4)$$

$$\begin{aligned} & \text{Calibration coefficient of channel } j, c_j (\text{g/impulse}) \\ & = \frac{\text{The number of represented sieve size classes of channel } j}{\sum_{i=D_{jrl}}^{D_{jru}} \text{Mean impulse per unit mass in a sieve size class } i, I_{(1)i,j} (\text{impulses/g})} \end{aligned} \quad (5)$$

$Q_{s-estimate}$ = Estimated mass of bedload for a sampling interval (g/sampling interval)

c_j = Calibration coefficients are functions of BSS in channel j , $f_j(\tau)$. (g/impulse)

τ = Mean bed shear stress (BSS) for a sampling interval (Pa)

I_j = Registered impulses for a sampling interval in channel j (impulses/sampling interval)

ε = Error caused by the difference between the detectable and the represented sieve size classes in all channels

equation (4) to experiment data is mainly due to differences between the detectable and representative sieve size class of channel j . Even though the mean impulses by BSS were reflected in the calibration coefficients, equation (4) is applicable only for low bedload transport rate conditions since multi-particle effects observed in the mixed-size particle experiments are negligible.

Table 8. Calibration coefficients from the individual particle experiments in three experimental hydraulic conditions

Bed Shear Stress, τ (Pa)	Calibration Coefficient, c_j (g/impulse)			
	$j = 1$	2	3	4
19.5	0.609	65.9	297	323
28.7	0.886	70.4	229	295
38.0	0.933	97.9	371	497

Convergence of the cumulative mean impulse frequency distributions is only met in channels 1 and 2. The calibration coefficients for channels 3 and 4 in Table 8 are based on the detectable particle sieve size classes of channels 3 and 4 rather than the represented particle sieve size classes. Data from channels 3 and 4 is excluded in the remaining portion of analysis since individual particle experiments were not conducted at high enough capacity bedload transport conditions to calibrate an equation with data from channels 3 and 4. The calibration coefficients for channels 1 and 2 are plotted in Figure 19 (a) and (b) with linear regression lines. Both a coefficient and a y-intercept of the linear regression equation for channel 2 are almost 100 times the regression equation for channel 1. The equations are similar with a factor of 100, but a closer view of the calibration coefficients regression line for channel 1 indicates a concave function, whereas calibration coefficients regression for channel 2 is a convex function. Thus, a firm conclusion for the correlation between calibration coefficients and BSS remains inconclusive until additional experimental hydraulic conditions are evaluated in future studies.

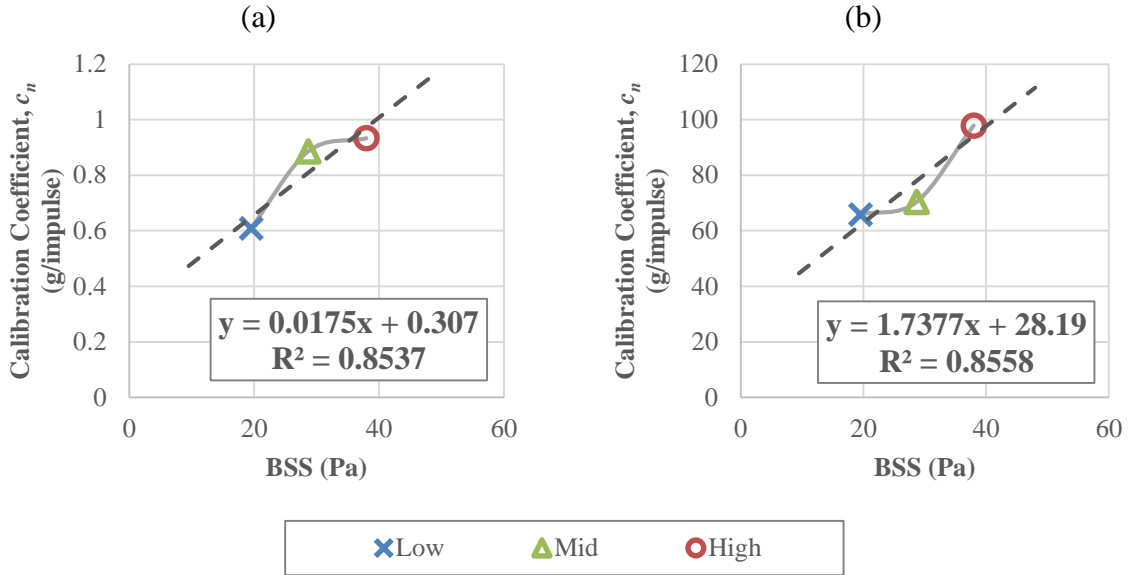


Figure 19. Calibration coefficient for the represented particle sieve size range in three experimental hydraulic conditions ((a) $j = 1$ and (b) 2)

According to the multi-size particle experiments in Figure 15, the bias between the predicted and the estimated mean impulses, β , increases with mean designed sediment-feeding rate in channel 1, whereas the bias in channel 2 is relatively constant. Figure 15 (a) and (b) are restructured in Figure 20 to directly compare the tendency of bias changed by the mean designed sediment-feeding rate, r , and BSS, τ . The estimated mean impulses from channel 1 are about 20% less than the predicted mean impulses in low hydraulic condition with $r = 1200$ g/min/0.2 m, and the bias increases up to approximately 100% with $r = 6000$ g/min/0.2 m. That is an indication of effects of multi-particle interaction and signal interference. Figure 20 shows the bias for channel 1 is small with $r = 1200$ g/min/0.2 m regardless of BSS and the bias for channel 2 is consistently small regardless of either BSS or mean designed sediment-feeding rate. These phenomena indicate that the number of particles have more influence on the bias rather than the total mass of particles.

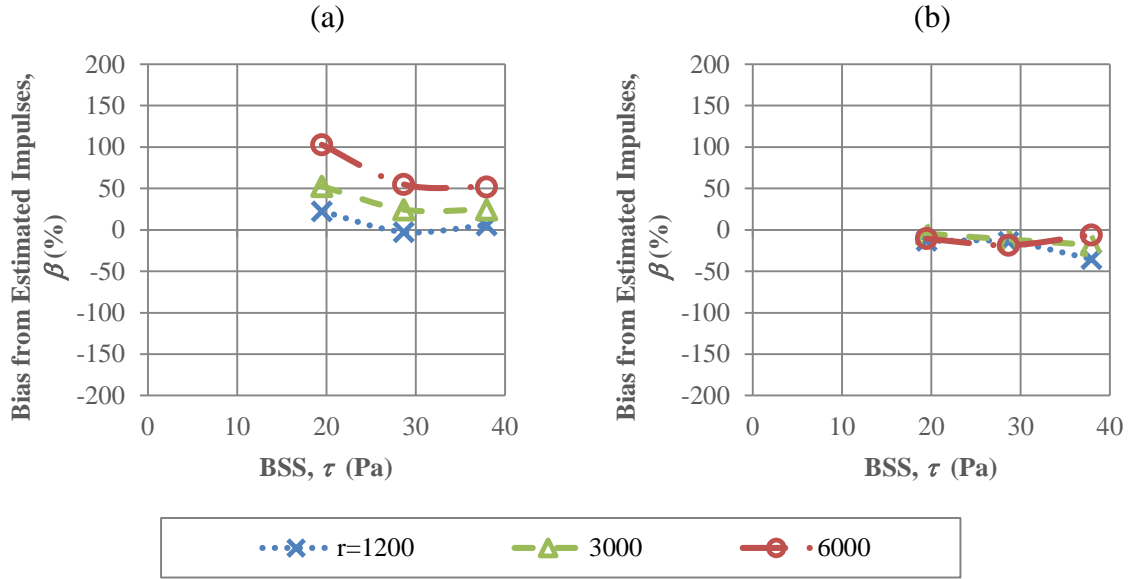


Figure 20. Bias of the predicted mean impulse from the estimated mean impulse changes by the mean designed sediment-feeding rate and BSS ((a) $j = 1$ and (b) 2)

As mentioned in the earlier chapter, the theoretical maximum number of impulses which can be registered for 60 seconds in the PBIS is about 15,000. Because of that, the closer the registered impulses become to the maximum capacity during a time period, the more dominant the influence of multi-particle signal interference becomes on the bias. In other words, the multi-particle signal interference becomes a more effective modifier on the bias with the increase of number of detectable particles in a certain channel j rather than the effect of multi-particle interaction on the mode of bedload particle motion. For that reason, as shown in Figure 15 (a), the estimated mean impulses in channel 1 show a similar tendency for the number of impulses at $r = 3000$ and 6000 g/min/0.2 m regardless of BSS and the predicted mean impulses. Furthermore, the estimated mean impulses of even under 1000 impulses per minute for channel 1 is still within the influence of multi-particle effects in all the experimental hydraulic conditions since in comparison to the bias in channel 2 the lowest bias in channel 1, -3% at $\tau = 28.7$ Pa and $r = 3000$ g/min/0.2 m, is still higher

than the highest bias in channel 2, -6 % at $\tau = 38.0$ Pa and $r = 6000$ g/min/0.2 m, in Figure 20 (a).

On the other hand, as shown in Figure 15 (b), the estimated mean impulses per minute on channel 2 are less than 70 even at the highest sediment-feeding rate, $r = 6000$ g/min/0.2 m. The estimated mean impulses in channel 2 are always higher than the predicted mean impulses but the absolute bias increases up to 35% at $\tau = 38.0$ Pa and $r = 1200$ g/min/0.2 m in Figure 20 (b). The negative bias when estimated mean impulses higher than the predicted mean impulses might be due to multi-particle effects as well. The negative bias in channel 2 could be caused by simultaneous impacts of particles passing through the 11.2 mm sieve size class, the lower boundary of detectable sieve size classes for channel 2. If that is in the case, the negative bias must decrease with the mean designed sediment-feeding rate which can increase the likelihood of simultaneous particle impacts, such as decrease of displacement distance. However, there are no significant increases of the estimated mean in channel 2 with the mean designed sediment-feeding rate in any experimental hydraulic conditions. Thus, additional analysis must be performed in a future study to clarify the negative bias such as comparison of time duration above the threshold of channel 2 for the individual and the multi-size particle experiments.

In consideration of practicality of bedload measurement in the field, 100% bias only at $\tau = 38.0$ Pa and $r = 6000$ g/min/0.2 m in channel 1 might be negligible. However, it is difficult to ignore the multi-particle effects based on the limited lab experiments since the range of experimental parameters are not wide enough to simulate full-scale bedload transport in natural channels. Thus, the calibration coefficients, c_j , in equation (4) are replaced with the adjusted calibration coefficients, k_j , in equation (8). Equations (4) and (8)

have the same linear format but the adjusted calibration coefficient is developed in a different manner by considering multi-particle interaction and signal interference in channel j . The adjusted calibration coefficient is a function of BSS, τ , and mean impulse rate, R_j , and is composed of two main functions as shown in equation (6). One is the function of BSS to estimate the calibration coefficients, c_j , in Table 8, and another is a function of BSS and mean impulse rate to estimate the bias, β , between the predicted and the estimated mean impulses. The second function works as a sort of conversion factor from the observed or estimated impulses to the predicted impulses for a sampling interval as shown in equation (7). Simply the adjusted calibration coefficient, k_j , is to convert observed impulses registered in channel j for a sampling time interval to predicted impulses in no multi-particle effect condition, and then finally to a total mass of bedload particles in the represented sieve size classes of channel j using the calibration coefficients, c_j . Therefore, equation (8) is the same as equation (4) when the second function is for low bedload transport rate conditions where multi-particle effects are negligible. The time interval of mean impulse rate, R_j , is specified as one minute. The mean impulse rate, R_j , is registered impulses, I_j , during a sampling interval divided by the sampling interval in minute unit. The adjusted calibration coefficients for channels 1 and 2 from equation (6), k_1 and k_2 , are summarized as a 3×3 matrix format in Table 9 (a) and (b). The adjusted calibration coefficients, k_j , are summarized by sediment-feeding rate, r , rather than mean impulse rate, R_j , in Table 9 since each k_j has a different R_j value.

Equation (9) is a general format of second-degree polynomial response surface equation, and can be developed to estimate the adjusted calibration coefficients for channels 1 and 2, k_1 and k_2 . Equation (9) is a function of two independent variables, mean

$$k_j = c_j \cdot \beta_j = f_j(\tau) \cdot g_j(\tau, R_j) = (f_j \cdot g_j)(\tau, R_j) \quad (6)$$

$$P_j = \beta_j \cdot I_j = g_j(\tau, R_j) \cdot I_j \quad (7)$$

$$Q_{s-estimate} = k_1 I_1 + k_2 I_2 - \varepsilon \quad (8)$$

k_j = Adjusted calibration coefficients of c_j considering bias caused by multi-particle interaction and signal interference. Functions of BSS and mean impulse rate in channel j (g/impulse)

c_j = Calibration coefficients are functions of BSS in channel j , $f_j(\tau)$. (g/impulse)

β_j = Bias between the predicted and the estimated impulses in channel j

τ = Mean bed shear stress (BSS) for a sampling interval (Pa)

R_j = Mean impulse rate in channel j during a sampling interval (impulses/minute)

P_j = Predicted impulses for a sampling interval in channel j (impulses/sampling interval)

$Q_{s-estimate}$ = Estimated mass of bedload for a sampling interval (g/sampling interval)

I_j = Registered impulses for a sampling interval in channel j (impulses/sampling interval)

ε = Error caused by the difference between the detectable and the represented sieve size classes in all channels

impulse rate, R_j and BSS, τ , which is developed from equation (8) using response surface methodology (RSM). Response surface models are developed based on nine adjusted calibration coefficients input data in each matrix. Thus, equation (9) does not seem to be composed of two separate equations as shown in equation (6). However, the calibration coefficients, c_j , and a converting equation from the estimate to the predicted mean impulses,

$g_j(\tau, R_j)$, are included in a quadratic function of mean impulse rate, R_j and BSS, τ , in equation (9).

**Table 9 (a). Adjusted calibration coefficient matrix for channel 1, k_1
(3 experimental hydraulic conditions \times 3 designed sediment-feeding rates)**

		Mean Designed Sediment-feeding Rate, r (g/min/0.2 m)		
		$r = 1200$	3000	6000
Bed Shear Stress, τ (Pa)	$\tau = 19.5$	0.746	0.930	1.237
	28.7	0.862	1.104	1.373
	38.0	0.986	1.162	1.417

**Table 9 (b). Adjusted calibration coefficient matrix for channel 2, k_2
(3 experimental hydraulic conditions \times 3 designed sediment-feeding rates)**

		Mean Designed Sediment-feeding Rate, r (g/min/0.2 m)		
		$r = 1200$	3000	6000
Bed Shear Stress, τ (Pa)	$\tau = 19.5$	57.21	62.93	58.98
	28.7	60.28	62.32	57.45
	38.0	63.50	80.35	92.15

The surface equation coefficients, a through f, for channels 1 and 2 are tabulated under equation (9). The 95% confidence boundaries of coefficients are also summarized beside the coefficients. The fitting criteria of each second-order polynomial response surface model for k_1 and k_2 are summarized in Table 10.

$$k_j = f_j(\tau) \cdot g_j(\tau, R_j) = (f_j \cdot g_j)(\tau, R_j) = a + b\tau + cR_j + d\tau^2 + e\tau R_j + fR_j^2 \quad (9)$$

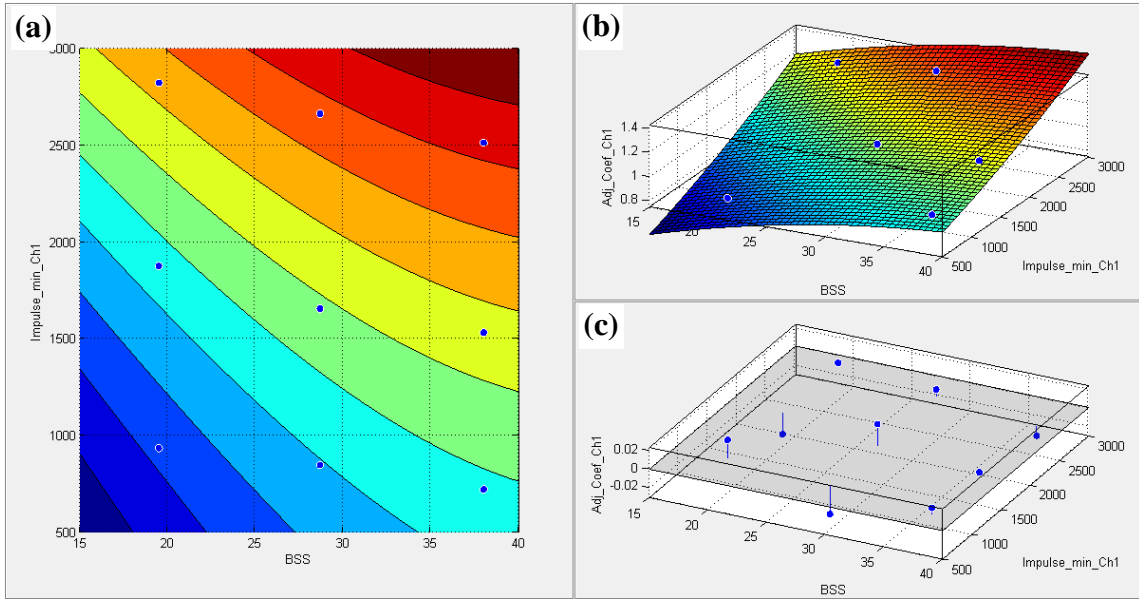
Coefficient	Channel 1	95% Confidence Bounds	Channel 2	95% Confidence Bounds
a	-0.1053	(-0.8896, 0.6789)	122.4	(-66.82, 311.6)
b	0.04236	(-0.005839, 0.09057)	-6.038	(-18.06, 5.981)
c	0.0001678	(-0.0002177, 0.0005534)	0.618	(-2.975, 4.211)
d	-0.0004546	(-0.001252, 0.0003422)	0.1119	(-0.08392, 0.3076)
e	-2.024 e-7	(-6.235 e-6, 5.83 e-6)	0.01879	(-0.05088, 0.08847)
f	2.806 e-8	(-5.309e-8, 1.092e-7)	-0.01288	(-0.04233, 0.01658)

Table 10. Goodness of fit

Channel	SSE	R-square	Adjusted R-square	RMSE
1	0.002708	0.9936	0.9828	0.03005
2	145.7	0.8734	0.6625	6.969

The graphical comparison between estimated k_j and predicted k_j for each channel 1 and 2 is performed in Figures 21 and 22. The value of R-square for k_I is 0.9936 in Table 10. The maximum error of k_I from the estimated k_I is -0.03 at $(\tau: 28.7, R_j: 1657)$ in Figure 21 (c) and is about -3.4%. As shown in Figure 21 (a) and (b), the contours for k_I show a linear-like increase from the bottom left to the top right. The estimated k_I fits a first-order plane response surface with R-square 0.9782. The maximum error of k_I from the first-order plane response surface is only -0.05 at $(\tau: 19.5, R_n: 1877)$. Therefore, either a first- or a second-order polynomial surface equation is precise enough over the range of experimental parameters. In this case, additional estimate points outside the range of experimental set-up are integral to verify which model is a better fit between either a first- or second-order polynomial response surface. However, a combined function, $(f_j \cdot g_j)(\tau, R_j)$, made by

multiplication of two functions of τ , $f_j(\tau)$ and $g_j(\tau, R_j)$, is mathematically a second or higher order function of τ if τ and R_j are independent from each other. Thus, the second-order polynomial response surface model is selected for channel 1.

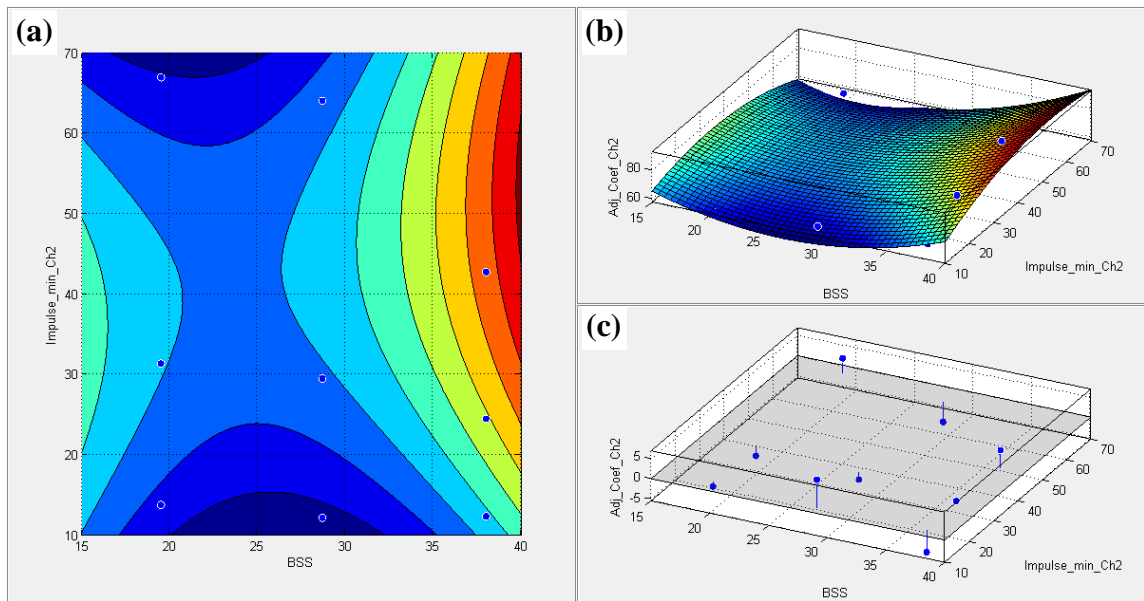


$$k_1 = -0.1053 + 0.04236\tau + 1.678 \times 10^{-4}R_1 - 4.546 \times 10^{-4}\tau^2 - 2.024 \times 10^{-7}\tau \cdot R_1 + 2.806 \times 10^{-8}R_1^2$$

Figure 21. Response surface model for channel 1 (a) contour, (b) surface and (c) residual plots

The R-square for k_2 is comparatively lower than for k_1 as shown in Table 10, but the goodness of fitting for k_2 is high with R-square 0.8734. Regardless of the statistical fitting criteria, a radical change of trend in k_2 appears around $\tau = 35$ Pa as shown in Figure 22 (a). The response surface of k_2 can be separated to the left and right based on visual observation of radical slope change. The left side of the surface has almost a constant k_2 regardless of τ or R_j . On the left side surface, the largest difference among the estimated k_2

is 5.7 in the direction of x-axis and 3.1 in the direction of y-axis. The maximum error from the estimated k_2 is 6.86 at (τ : 28.7, R_2 : 12) in Figure 22 (c). On the other hand, the right side of the response surface shows an apparent change of trend similar to the trend of k_1 increasing from the bottom left to the top right linearly in Figure 21 (a). The largest difference among the estimated k_2 on the right side surface is larger than on the left side surface with a difference of 28.6 in the direction of the y-axis. The maximum error from the estimated k_2 is smaller than on the left side surface with a value of -5.4. According to the comparison between the left and right sides of the response surface, the visual transition of the response surface around $\tau = 35$ Pa is evident. Thus, the prediction of k_2 with the response surface equation in Figure 22 seems to be limited in the range of current



$$k_2 = 122.4 - 6.038 \tau + 0.618 R_2 + 0.1119 \tau^2 + 0.01879 \tau \cdot R_2 - 0.01288 R_2^2$$

Figure 22. Response surface model for channel 2 (a) contour, (b) surface and (c) residual plots

experimental parameters. Extrapolation of k_2 with the equation has limited value due to lack of calibration data and additional observation points outside the range of current experimental parameters are required.

The quantitative comparison between the actual sediment mass used in the experiments and the estimated sediment mass from equation (8) and (9) is summarized in Table 11. Even though the equations for k_j are derived from the experiments, this calibration model usually overestimates the mass of bedload to some degree due to two inherent error factors associated with the bedload estimation method. The first error factor is the difference in particle size classes. The test gravels are classified by the half-phi (ϕ) scale sieve size classes, but estimated sediment is classified by only 2 threshold channels of the PBIS determined by the represented sieve size classes of channels 1 and 2. Another overestimate error factor is the difference between the detectable and the represented sieve size classes in channel j . The calibration coefficients, c_j , are estimated by mean mass of

Table 11. Estimate error of bedload quantity

Mean Bed Shear Stress, τ (Pa)	Designed Sediment-feeding Rate, Q_{s-feed} (g/s/0.2 m)	Actual Mass of Sediment, $Q_{s-actual}$ (g)		Adjusted Calibration Coefficient, k_j (g/impulse)		Estimated Mass of Sediment, $Q_{s-estimate}$ (g)		% Error between Actual and Estimated Mass, ε		
		Ch1	Ch2	Ch1	Ch2	Ch1	Ch2	Ch1	Ch2	Combined
19.5	20	300	300	0.73	58.36	340	403	13.2	34.2	23.7
	50			0.95	65.42	358	410	19.4	36.8	28.1
	100			1.23	55.41	348	371	16.1	23.6	19.9
28.7	20			0.89	53.46	379	326	26.3	8.7	17.5
	50			1.08	64.17	358	379	19.3	26.2	22.8
	100			1.37	62.53	364	400	21.3	33.4	27.3
38.0	20			0.98	69.00	354	428	17.9	42.6	30.2
	50			1.16	79.36	355	389	18.5	29.6	24.0
	100			1.43	87.84	359	375	19.6	25.1	22.4

Particles in the represented sieve size classes, but the registered impulses in channel j are generated by all detectable particles over the upper boundary sieve size.

The range of sieve size classes of multi-size experiment sediment samples cover the entire represented sieve size classes for channel 1 but only partially cover the represented sieve size classes for channel 2. Therefore, the overestimate in channel 1 is caused only by the second error factor, whereas the overestimate in channel 2 is caused by both error factors. This may explain why the error in channel 2 is generally larger than in channel 1. The mean overestimate rate with the multi-size experiment sediment sample is about 24% as shown in Figure 23. The error rate has an evident linear tendency regardless of either τ or r .

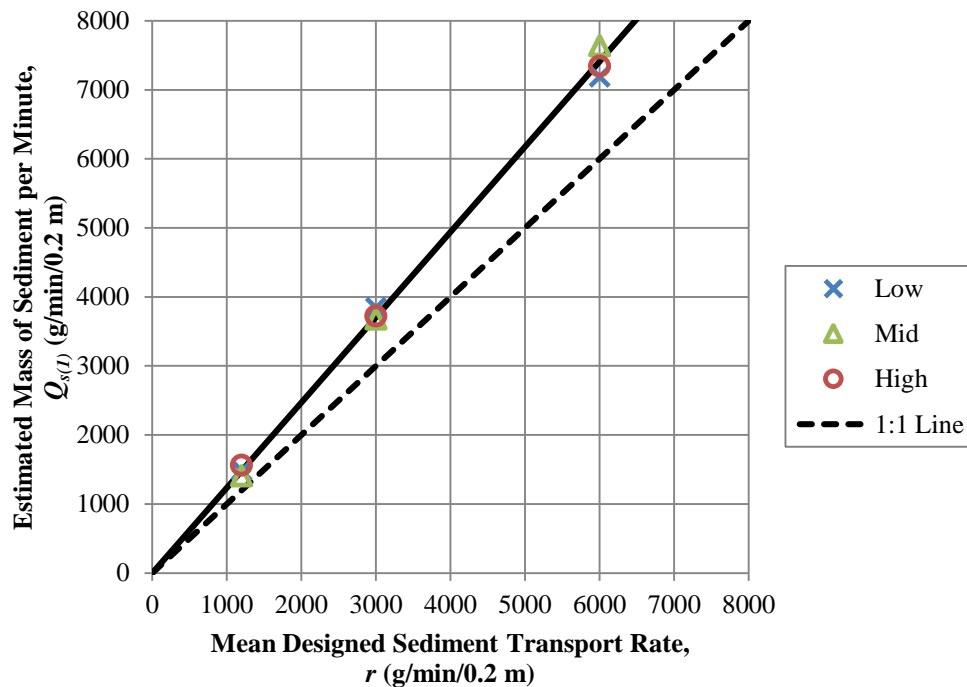


Figure 23. Comparison between mean designed sediment transport rate of multi-size particle sample and estimated sediment transport rate using the bedload estimate model for the multi-channel PBIS

The comparison of particle size frequency distribution in Figure 24 reconfirms the first inherent error factor of this bedload estimation model. Dashed lines in Figure 24 (a)–(c) indicate the actual cumulative particle size frequency distribution of multi-size experiment sediment sample. Three solid lines in each graph indicate the cumulative estimated particle size frequency distributions for the 3 mean sediment-feeding rates for experimental hydraulic conditions. The lower section of the solid line is the represented sieve size range of channel 1, and the upper section is the represented sieve size range of channel 2. The largest sieve size class for the actual multi-size experiment sediment sample is 22.5 mm, but the upper boundary of the represented sieve size range of channel 2 is 32 mm. Thus, when the actual sediment particle sieve size range partially cover the represented particle sieve size range as shown in Figure 24, the estimated particle size frequency distributions from the bedload estimate model are coarser than the actual particle size frequency distributions. However, due to a larger error in a higher threshold channel 2, the estimated particle size frequency distribution in a lower threshold channel 1 relatively has a smaller error in the cumulative frequency distribution and becomes closer to the actual particle size frequency distribution at the 11.2 mm passing sieve size class.

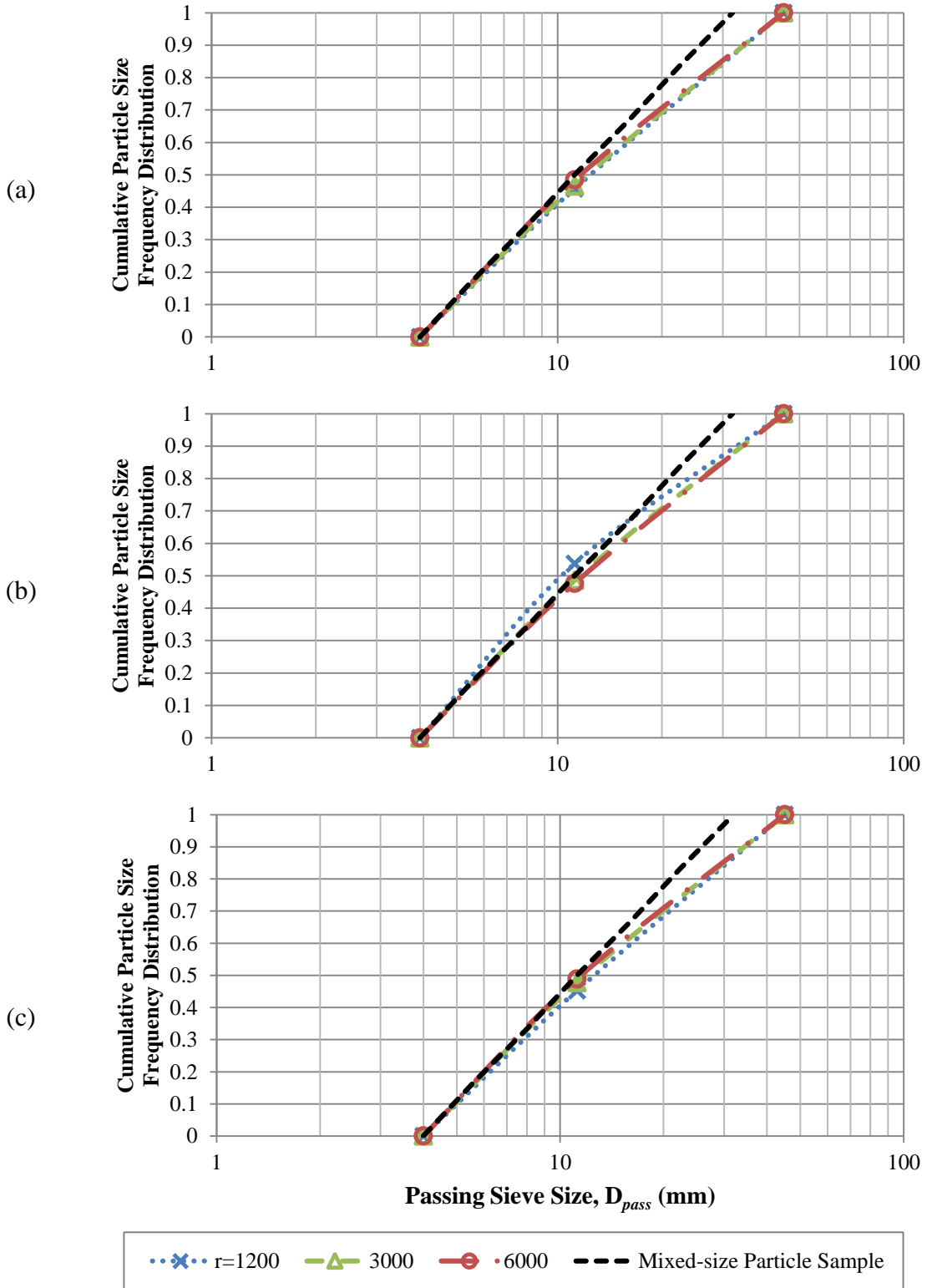


Figure 24. Comparison of cumulative particle-size distribution of equal size-fraction experimental sediment sample with estimated particle-size distributions in three hydraulic conditions ($\tau =$ (a) 19.5 Pa, (b) 28.7 Pa and (c) 38.0 Pa)

CHAPTER VI. CONCLUSION

The multi-channel PBIS facilitates continuous local-scale monitoring of bedload in natural streams by detecting impacts of sediment particles on the device sensor and recording impact strength and frequency. Use of the PBIS device provides many advantages over traditional techniques that can typically require physical capture of sediment particles using in-stream containers and require on-site retrieval of sediment particles for evaluation. The PBIS provides a means for efficient in-situ sediment monitoring simultaneously at many stream cross-sections over a comparatively long-term period with minimal intervention. On the perspective of practicality in field bedload monitoring, these features provide an unquestioned advantage. The cost-effectiveness of the PBIS must balance a choice between monitoring many sites with a possibly less accurate and higher device costs and lower labor or installation costs, versus the more economical device costs, monitoring fewer sites with accurately calibrated devices, and higher personnel costs. Even though neither technique can be entirely overlooked, engineers, scientists and river managers must select a bedload measurement technique compatible with their purposes. The PBIS has an unquestioned advantage for the former.

The common disadvantages of surrogate bedload measurement devices, such as the PBIS, are the calibration process necessary to quantify the detection signal to the bedload mass and possible additional direct sampling to determine particle size frequency distribution. To investigate this technique in further detail, a multi-channel PBIS was developed to estimate bedload particle size frequency distribution as well as total sediment

bedload mass. According to analytical results, particle size detection by the magnitude of particle impact energy on the PBIS appears reliable with strong correlation. However, the variance of peak signal by particles, even within the same sieve size class, is large. To determine particle size distribution and mass of bedload with constant sensor detection thresholds, the proposed calibration model includes two parameters, bed shear stress, τ and mean impulse rate, R_j . However, additional field measurements are required to determine the practical reliability of bedload estimates using the PBIS in natural stream channels.

This bedload estimate model for the multi-channel PBIS was developed based on the laboratory experiments conducted in a controlled environment with many assumptions. Moreover, the experiment scale was limited by the capacity of equipment as well. Thus, this model might be sufficient only to apply for comparatively low to moderate bedload transport rate conditions at low to moderate slope channels where small gravels are dominant on the channel bed. However, the experiment and analysis provide a direction for improvement and illustrate the feasibility of field measurement in natural streams with a multi-channel PBIS. Collecting field data in natural streams and large-scale lab experiments capable of transporting larger sediment particles and thereby activating higher threshold sensor channels is a direction of future study.

REFERENCES

- Anderson, M. G. (1976). An inexpensive circuit design for the acoustic detection of oscillations in bedload transport in natural streams. *Earth Surface Processes*, 1(3), 213-217.
- Bänziger, R., and Burch, H. (1990). Acoustic sensors (hydrophones) as indicators for bed load transport in a mountain torrent. In H. Lang and A. Musy (Eds.), *Hydrology in Mountainous Regions I-Hydrological Measurements; The Water Cycle* (Vol. IAHS Publication No. 193, pp. 207–214): International Association of Hydrological Sciences.
- Bunte, K., and Abt, S. R. (2001). *Sampling surface and subsurface particle-size distributions in wadable gravel-and cobble-bed streams for analyses in sediment transport, hydraulics, and streambed monitoring*. (Gen. Tech. Rep. RMRS-GTR-74). Fort Collins, CO: U.S. Dept. of Agriculture, Forest Service, Rocky Mountain Research Retrieved from http://www.fs.fed.us/rm/pubs/rmrs_gtr074.html.
- Cantrell, W., Schwartz, J., and Barry, W. (2009). *Bedload Composition and Development of 2D Stream Sediment Model for Stream Restoration Design Applications in Urbanizing Watersheds*. Paper presented at the World Environmental and Water Resources Congress 2009.
- Diplas, P., Kuhnle, R., Gray, J., Glysson, D., and Edwards, T. (2008). Sediment Transport Measurements. In M. H. García (Ed.), *Sedimentation engineering : processes, measurements, modeling, and practice* (pp. 307-353). Reston, Va.: American Society of Civil Engineers.
- F. Douglas Shields, J., Copeland, R. R., Klingeman, P. C., Doyle, M. W., and Simon, A. (2003). Design for Stream Restoration. *Journal of Hydraulic Engineering*, 129(8), 575-584.
- Gomez, B. (1991). Bedload transport. *Earth-Science Reviews*, 31(2), 89-132.
- Gomez, B. (2006). The potential rate of bed-load transport. *Proceedings of the National Academy of Sciences*, 103(46), 17170-17173.
- Gomez, B., and Church, M. (1989). An assessment of bed load sediment transport formulae for gravel bed rivers. *Water Resour. Res.*, 25(6), 1161-1186.

- Gray, J. R., Laronne, J. B., and Marr, J. D. G. (2010). Bedload-surrogate monitoring technologies: U.S. Geological Survey Scientific Investigations Report 2010–5091. 37 p.
- Gray, J. R., and Simões, F. J. M. (2008). Estimating sediment discharge, appendix D In M. Garcia (Ed.), *Sedimentation engineering-Processes, measurements, modeling, and practice* (pp. 1067-1088): American Society of Civil Engineers.
- Hayward, J. A. (1978). *Hydrology and stream sediments in a mountain catchment*. (Doctor of Philosophy), University of Canterbury.
Retrieved from <http://hdl.handle.net/10182/1653>
- Hubbell, D. W. (1964). *Apparatus and techniques for measuring bedload*. Washington: U.S. Govt. Print. Off.
- Johnson, P., and Muir, T. C. (1969). Acoustic Detection Of Sediment Movement. *Journal of Hydraulic Research*, 7(4), 519-540.
- Khorram, S., and Ergil, M. (2010). Most Influential Parameters for the Bed-Load Sediment Flux Equations Used in Alluvial Rivers1. *JAWRA Journal of the American Water Resources Association*, 46(6), 1065-1090.
- Meade, R. H., Yuzyk, T. R., and Day, T. J. (1990). Movement and storage of sediment in rivers of the United States and Canada. In M. G. Wolman and H. C. Riggs (Eds.), *Surface water hydrology* (pp. 255–280). Boulder, CO: Geological Society of America.
- Møen, K. M., Bogen, J., Zuta, J. F., Ade, P. K., and Esbensen, K. (2010). Bedload Measurement in Rivers Using Passive Acoustic Sensors. In *Bedload-surrogate Monitoring Technologies*, Gray JR, Laronne JB, Marr JDG (eds), *US Geological Survey Scientific Investigations Report 2010–5091*. US Geological Survey: Reston, VA; 296–318., 336-351.
- Papanicolaou, A., Elhakeem, M., Krallis, G., Prakash, S., and Edinger, J. (2008). Sediment Transport Modeling Review—Current and Future Developments. *Journal of Hydraulic Engineering*, 134(1), 1-14.
- Pitlick, J., Cui, Y., and Wilcock, P. R. (2009). *Manual for computing bed load transport using BAGS (Bedload Assessment for Gravel-bed Streams) software*. Fort Collins, Colo.: U.S. Dept. of Agriculture, Forest Service, Rocky Mountain Research Station
Retrieved from <http://purl.access.gpo.gov/GPO/LPS117587>.
- Pitlick, J., and Wilcock, P. (2001). Relations between Streamflow, Sediment Transport, and Aquatic Habitat in Regulated Rivers. In J. M. Dorava, D. R. Montgomery, B. B. Palcsak and F. A. Fitzpatrick (Eds.), *Geomorphic Processes and Riverine Habitat* (pp. 185-198). Washington, D. C.: American Geophysical Union.

- Richards, K. S., and Milne, L. M. (1979). Problems in the calibration of an acoustic device for the observation of bedload transport. *Earth Surface Processes*, 4(4), 335-346.
- Richardson, K., Benson, I., and Carling, P. A. (2003). An instrument to record sediment movement in bedrock channels. *IAHS publication.*, 283, 228-235.
- Rickenmann, D., and Fritschi, B. (2010). Bedload Transport Measurements Using Piezoelectric Impact Sensors and Geophones. In *Bedload-surrogate Monitoring Technologies*, Gray JR, Laronne JB, Marr JDG (eds), US Geological Survey Scientific Investigations Report 2010–5091. US Geological Survey: Reston, VA; 296–318., 407-423.
- Rickenmann, D., and McArdell, B. W. (2007). Continuous measurement of sediment transport in the Erlenbach stream using piezoelectric bedload impact sensors. *Earth Surface Processes and Landforms*, 32(9), 1362-1378.
- Rickenmann, D., and McArdell, B. W. (2008). Calibration of piezoelectric bedload impact sensors in the Pitzbach mountain stream. *Geodinamica Acta*, 21(1), 35.
- Rickenmann, D., Turowski, J. M., Fritschi, B., Klaiber, A., and Ludwig, A. (2012). Bedload transport measurements at the Erlenbach stream with geophones and automated basket samplers. *Earth Surface Processes and Landforms*, 37(9), 1000-1011.
- Ryan, S. E., Bunte, K., and Potyondy, J. P. (2005, September 9–11, 2003). *Breakout session II, bedload-transport measurement: Data needs, uncertainty, and new technologies*. Paper presented at the Proceedings of the Federal Interagency Sediment Monitoring Instrument and Analysis Research Workshop, September 9–11, 2003, Flagstaff, Arizona, Flagstaff, Arizona.
- Schwendel, A. C., Death, R. G., and Fuller, I. C. (2010). The assessment of shear stress and bed stability in stream ecology. *Freshwater Biology*, 55(2), 261-281.
- Wilcock, P., Pitlick, J., and Cui, Y. (2009). *Sediment transport primer: estimating bed-material transport in gravel-bed rivers*. (Gen. Tech. Rep. RMRS-GTR-226). Fort Collins, CO: U.S. Dept. of Agriculture, Forest Service, Rocky Mountain Research Station Retrieved from http://www.fs.fed.us/rm/pubs/rmrs_gtr226.html.

APPENDIX

LIST OF NOTATIONS AND UNITS

$f_j(x)$ and $g_j(x)$	Mathematical function of x in channel j	-
$1/2-\phi$ or ϕ	Particle sieve size class scale (refer to Table 1)	-
a, b, c, d, e and f	Regression equation coefficients	-
c_j	Calibration coefficient of channel j	g/impulse
D_{pass}	Passing sieve size	mm
D_{ret}	Retaining sieve size	mm
D_{jrl}	Lower boundary of represented sieve size classes in channel j	mm
D_{jru}	Upper boundary of represented sieve size classes in channel j	mm
β_j	Bias between the predicted and the estimated impulses in channel j	-
ε_{a-e}	Estimate error of sediment transport	g
i	Retained particle sieve size class order in $1/2-\phi$ scale beginning from $\phi = -2$ ($D_{ret} = 4$ to 64 mm)	1 to 9
$I_{(1)i,j}$	Mean impulses per unit mass (= 1 g) of channel j in a sieve size class i	impulse/g
$I_{(600)1-6,j}$	Mean impulses per 600 g multi-size sample $i = 1$ to 6	-
$I_{(p)i,j}$	Mean impulses per i -sieve size class particle registered in channel j	impulse/particle
$I_{1-6,j(1),r}$	Estimated mean impulses per minute with mean sediment-feeding rate of multi-size sample $i = 1$ to 6	-

$I_{i,j}$	Total registered impulses in channel j by particles in a sieve size class i	-
I_j	Registered impulses in channel j for a sampling time interval	impulse
j	Threshold channel number	1 to 4
k_j	Adjusted calibration coefficient of channel j	g/impulse
$m_{(p)i}$	Mean particle mass in a sieve size class i	g/particle
$N_{(1)i}$	Mean number of particles per unit mass (= 1 g) in a sieve size class i	particle/g
$N_{(100)i}$	Mean number of test particles in 100g particle sample in a sieve class i	-
$N_{(p)i}$	Number of test particles	-
$N_{(reg)i}$	Number of particles registered in a sieve size class i	-
$P_{(100)i,j}$	Predicted mean impulses per 100g in a sieve class	-
$P_{(600)1-6,j}$	Predicted mean impulses per 600g multi-size sample $i = 1$ to 6	-
$P_{1-6,j(1),r}$	Predicted mean impulses per minute with mean sediment-feeding rate of multi-size sample $i = 1$ to 6	-
$P_{1-6,j(1),r}$	Predicted mean impulses per minute with mean sediment-feeding rate of multi-size sample $i = 1$ to 6	-
P_j	Predicted impulse in channel j	-
Q	Mean discharge	L/s
Q_s	Total mass of sediment transport	g
$Q_{s(1)}$	Estimated mass of sediment per minute	g/min/0.2m
$Q_{s-actual}$	Actual mass of sediment transport	g
$Q_{s-estimate}$	Estimated mass of sediment transport	g
Q_{s-feed}	Mean sediment-feeding rate	g/s/0.2m
r	Mean sediment-feeding rate	g/min/0.2m

$r_{(reg)i}$	Mean particle registration rate in a sieve size class i	%
R_j	Mean impulse rate in channel j	impulse/minute
τ or BSS	Mean bed shear stress	Pa
t_{s-feed}	Mean sediment-feeding duration	second
v	Mean velocity	m/s

CURRICULUM VITAE

NAME: Jeong Won Park

ADDRESS: Department of Civil and Environmental Engineering
University of Louisville
101 W.S. Speed Hall
Louisville, KY 40292

DOB: Seoul, Republic of Korea – August 13, 1977

EDUCATION and TRAINING B.S., Civil and Environmental Engineering
University of Louisville
1997-2001

M.Eng., Civil and Environmental Engineering
University of Louisville
2002-2007

Ph.D., Civil and Environmental Engineering
University of Louisville
2007-2013

PROFESSIONAL CERTIFICATES and LICENSES Engineer in Training (EIT): EIT No. 14057
Issued on December 27, 2010

Land Surveyor in Training (LSIT): LSIT No. 1981
Issued on May 12, 2011

Professional Engineer (PE) in Kentucky: License No. 28344
Issued on December 22, 2011

PUBLICATIONS and PRESENTATIONS PharmaSUG 2008 proceedings: Public Health Research, Atlanta, Georgia
“Using SAS® Enterprise Guide 4.0® to find a Correlation between Mortality and Co-morbidities for Prostate Disease Patients”

2008 SAS Business Forecasting Conference: Poster Presentation,
Cary, North Carolina
“Hydrologic Time Series Modeling with Domain Knowledge for
Whitemarsh Run at White Marsh, MD (Feb. 1959 ~ Sept. 2006)”